European Journal of Medicinal Chemistry 84 (2014) 404–416

Contents lists available at ScienceDirect

European Journal of Medicinal Chemistry

journal homepage: http://www.elsevier.com/locate/ejmech

Original article

Synthesis and pharmacological evaluation of 6-aminonicotinic acid analogues as novel $GABA_A$ receptor agonists

Jette G. Petersen [a], Troels Sørensen [b], Maria Damgaard [a], Birgitte Nielsen [a], Anders A. Jensen [a], Thomas Balle [b], Rikke Bergmann [a], Bente Frølund [a, *]

[a] Department of Drug Design and Pharmacology, Faculty of Health and Medical Sciences, University of Copenhagen, Universitetsparken 2, DK 2100 Copenhagen, Denmark

[b] Faculty of Pharmacy, The University of Sydney, Camperdown Campus, 2006 NSW, Australia

ARTICLE INFO

Article history:
Received 1 May 2014
Received in revised form
10 July 2014
Accepted 11 July 2014
Available online 11 July 2014

Keywords:
GABA-A receptor agonists
Structure–activity studies
2-Aminonicotinic acid analogues

ABSTRACT

A series of 6-aminonicotinic acid analogues have been synthesized and pharmacologically characterized at native and selected recombinant $GABA_A$ receptors. 6-Aminonicotinic acid (**3**) as well as 2- and 4-alkylated analogues (**9**–**11**, **14**–**16**) display low to mid-micromolar $GABA_AR$ binding affinities to native $GABA_A$ receptors (K_i 1.1–24 μM). The tetrahydropyridine analogue of **3** (**22**) shows low-nanomolar affinity (K_i 0.044 μM) and equipotency as an agonist to GABA itself as well as the standard $GABA_A$ agonist isoguvacine. Cavities surrounding the core of the GABA binding pocket were predicted by molecular interaction field calculations and docking studies in a $\alpha_1\beta_2\gamma_2$ $GABA_A$ receptor homology model, and were confirmed by affinities of substituted analogues of **3**. The tight steric requirements observed for the remarkably few $GABA_AR$ agonists reported to date is challenged by our findings. New openings for agonist design are proposed which potentially could facilitate the exploration of different pharmacological profiles within the $GABA_AR$ area.

1. Introduction

γ-Aminobutyric acid (GABA) is the major inhibitory neurotransmitter in the central nervous system (CNS) where it exerts its effects through ionotropic ($GABA_A$) receptors resulting in fast synaptic inhibition and metabotropic ($GABA_B$) receptors resulting in slow, prolonged inhibitory signals. The GABA neurotransmitter system is essential for the overall balance between neuronal excitation and inhibition and known to be implicated in many disorders such as anxiety, epilepsy, mood and cognitive disorders, insomnia, and schizophrenia [1,2].

The $GABA_A$ receptors ($GABA_ARs$) belong to the Cys-loop superfamily of ligand-gated ion channels also comprising the nicotinic acetylcholine receptors, 5-HT_3 serotonin receptors, and glycine receptors. The assembled receptor complex is a circular arrangement of five subunits making up a chloride selective ion-conducting channel. 19 different human $GABA_A$ subunits have been identified; α_{1-6}, β_{1-3}, γ_{1-3}, δ, ε, θ, π, and ρ_{1-3}, and these subunits combine in different stoichiometries, the most common ones being 2α-2β-1γ heteropentamers [3]. From the at least 26 native $GABA_A$ receptors subtypes proposed, the predominant combinations are believed to be $\alpha_1\beta_2\gamma_2$, $\alpha_2\beta_3\gamma_2$, and $\alpha_3\beta_3\gamma_2$ [4]. $GABA_ARs$ composed of ρ subunits, also designated $GABA_CRs$ due to their distinct physiological and pharmacological properties, assemble as homopentameric or pseudohomomeric receptors [5].

Typical orthosteric $GABA_AR$ agonists contain both basic and acidic functionalities positioned in a narrow distance range from each other and are in general relatively small molecules [6]. These $GABA_A$ agonists include the highly potent natural product compound muscimol [7,8], 4,5,6,7-tetrahydroisoxazol [5,4-*c*]pyridin-3-ol (THIP) [9], 1,2,3,6-tetrahydropyridine-4-carboxylic acid (isoguvacine), piperidine-4-carboxylic acid (isonipecotic acid) [8], and 5-(4-piperidyl)-3-isoxazolol (4-PIOL) [10,11] (Fig. 1). In general, studies have shown that the introduction of even small substituents onto a $GABA_A$ agonist, such as muscimol and THIP, is

Abbreviations: 4-PIOL, 5-(4-piperidyl)-3-isoxazol; DCVC, dry column vacuum chromatography; ELIC, *Erwinia* ligand-gated ion channel; FC, flash chromatography; FLIPR, fluorescent imaging plate reader; FMP, FLIPR membrane potential; GABA, γ-aminobutyric acid; GLIC, *Gloeobacter* ligand-gated ion channel; GluCl, glutamate-gated ion channel; IFD, induced fit docking; RP-FC, reverse phase flash chromatography; THIP, 4,5,6,7-tetrahydroisoxazol[5,4-*c*]pyridine-3-ol.

* Corresponding author.
E-mail addresses: bfr@sund.ku.dk, bfr@farma.ku.dk (B. Frølund).

http://dx.doi.org/10.1016/j.ejmech.2014.07.039
0223-5234/

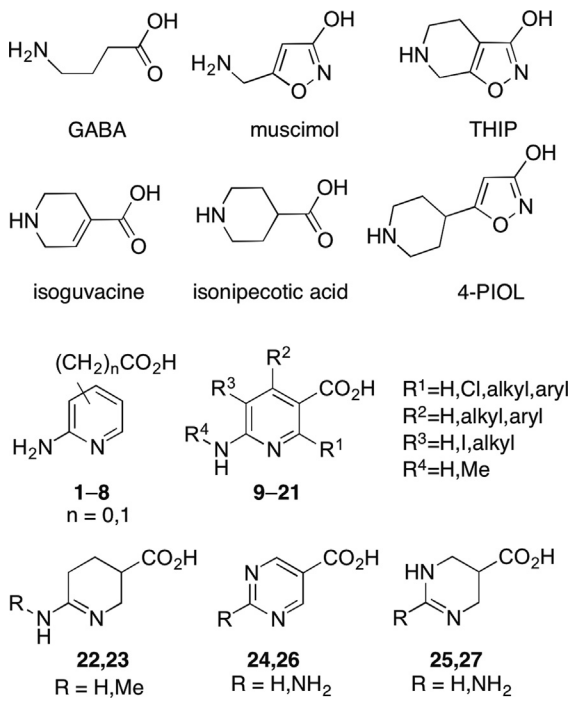

Fig. 1. Structures of $GABA_A$ agonists: GABA, muscimol, THIP, isoguvacine, isonipecotic acid, 4-PIOL and general structures of the 6-aminonicotinic acid analogues **1**–**27**.

detrimental for receptor activity indicating very limited space in the areas surrounding the core scaffolds of these agonists [6].

Classical medicinal chemistry and pharmacophore models have aided the insight into details of binding and function of these agonists [12,13]. As a high-resolution 3D structure of a $GABA_AR$ has yet to be published, rational ligand design is depending on homology models created from related templates with low amino acid sequence identities to the $GABA_AR$. These include X-ray structures of acetylcholine binding proteins (AChBPs) [14–16], full length receptor structures of the glutamate-gated chloride channel from *Caenorhabditis elegans* (GluCl) [17], and of the bacterial ion channels ELIC [18] and GLIC [19] from *Erwinia chrysanthemi* and *Gloeobacter violaceus*.

We have recently published homology models of the $GABA_A$ $\alpha_1\beta_2\gamma_2$ receptor based on these templates with both agonists [20] and antagonists bound [21]. The most notable difference between the agonist and antagonist models is the position of the hairpin shaped C-loop which is more open in the antagonist model to accommodate the larger antagonists. Furthermore, the functionally important α_1Arg66 is, as previously suggested [12,21], observed in two distinct conformations in the two models. The models have aided design of compounds and exploration of binding modes for a number of agonists [20] and antagonists [21] and have led to a better understanding of the architecture of the binding site, including the strict steric requirements for agonist binding as evident from the structure–activity relationships (SARs) of 4-aminomethyl-1-hydroxypyrazole analogues of muscimol [22]. However, the enhanced structural insight has not advanced the field of subtype selective $GABA_AR$ agonists.

Inspired by the abovementioned agonist model, we have explored 6-aminonicotinic acid (**3**) as a lead structure and developed of a series of novel $GABA_AR$ agonists (**9**–**27**) in order to challenge the limited structural diversity of $GABA_AR$ agonists and facilitate the quest for subtype selective $GABA_AR$ agonists. We report on the synthesis and pharmacological characterization at the $GABA_AR$ of a series of compounds containing 2-aminopyridine or analogous amidine/guanidine ring systems as novel amine bioisosteres.

2. Results

2.1. Chemistry

The series of 2-aminopyridines **1**–**8** with carboxylic acid substituents systematically placed around the pyridine ring were all commercially available except for 2-(2-aminopyridin-4-yl)acetic acid (**6**) which was synthesized from 4-methyl-2-aminopyridine (Scheme 1). *tert*-Butoxycarbonyl protection of the amine affording **28** was followed by lithiation of the methyl group using lithium diisopropylamide (LDA) and subsequent quenching with diethylcarbonate to give the ethyl ester **29**. Deprotection under basic conditions afforded the target compound **6**.

The synthetic procedures for the 6-aminonicotinic acid analogues (**9**–**21**) are depicted in Schemes 2–4. The methyl substituted analogues **9**, **14**, **19** (Scheme 2) were prepared from methyl-3-bromo-6-aminopyridines **30**–**32** using a palladium catalyzed cyanation [23] followed by acidic hydrolysis of the nitriles to the corresponding carboxylic acids. The 2-substituted analogues **10**–**13** (Scheme 3) were prepared from 2,6-dichloropyridine using nucleophilic aromatic substitution under high pressure to form 6-chloro-2-aminopyridine (**36**) [24]. Subsequent regioselective iodination with *N*-iodosuccinimide (NIS) [25] and palladium catalyzed cyanation afforded the central intermediate **38** serving as cross-coupling partner for the formation of 2-substituted analogues **39**–**41**. Ethyl and butyl groups were introduced via Negishi cross coupling with Et_2Zn or BuZnBr [26], and the phenyl group was introduced using Suzuki cross coupling with phenylboronic acid. The 4-substituted analogues **15**–**17** (Scheme 3) were prepared from commercially available 4-chloro-2-aminopyridine **42** in an analogous manner to the 2-substituted analogues. The conversion of **44** to **45** and **46** was performed with iron-catalyzed cross coupling with EtMgBr or BuMgBr [27] and to **47** by cross-coupling using phenylboronic acid. The Negishi cross coupling conditions applied for the synthesis of the 2-substituted **39** and **40** were unsuccessful for the formation of the 4-substituted compounds. The 5-position (Scheme 4) was accessed via iodination of commercially available methyl 6-aminonicotinate (**48**) with iodine and silver sulphate (Ag_2SO_4) [28]. The iodinated intermediate **49** was deprotected by acidic hydrolysis affording compound **18** [28] or subjected to Suzuki cross coupling with potassium vinyltrifluoroborate affording compound **50**. Selective hydrogenation of the double bond followed by deprotection by acidic hydrolysis afforded the 5-ethyl analogue **20**.

The aminotetrahydro -pyridine and -pyrimidine compounds **22** [29], **23** and **27** [29] were synthesized using catalytic hydrogenation over a PtO_2 catalyst starting from 6-aminonicotinic acid **3**, **21**, and **26**, respectively (Scheme 5). The synthesis of pyrimidine compound **24** [30] was achieved from 5-bromopyrimidine by

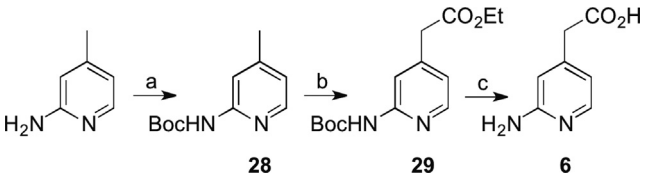

Scheme 1. Reagents and conditions: (a) Boc_2O, *tert*-BuOH, rt, (b) LDA, THF, −70 °C–0 °C, then diethylcarbonate, 0 °C, (c) 1 M aq. NaOH, MeOH, reflux.

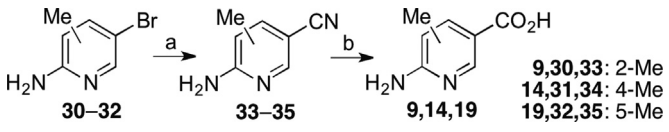

Scheme 2. Reagents and conditions; (a) $Zn(CN)_2$, $Pd_2(dba)_3$, dppf, DMF/H_2O 99:1, 120 °C, (b) 6 M or conc. HCl, reflux.

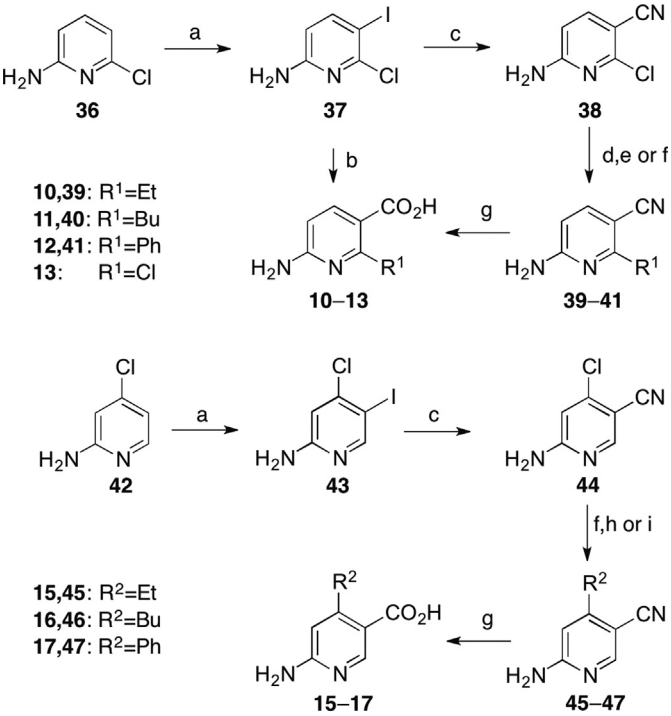

Scheme 3. Reagents and conditions; (a) NIS, DMF, rt, (b) 2.2 eq. nBuLi, THF/Et_2O, −110 °C, then CO_2 (gas), −110 °C to −30 °C, (c) $Zn(CN)_2$, $Pd_2(dba)_3$, dppf, DMF/H_2O 99:1, 120 °C, microwave irradiation, (d) Et_2Zn, $Pd_2(PPh_3)_4$, 1-methyl-2-pyrrolidinone (NMP), 100 °C, microwave irradiation, (e) BuZnBr, $Pd_2(PPh_3)_4$, NMP, rt, (f) $PhB(OH)_2$, $Pd_2(PPh_3)_4$, toluene/EtOH 10:1, 100 °C microwave irradiation, (g) Conc. HCl, reflux, (h) EtMgBr, $Fe(acac)_3$, NMP/THF 10:1, rt, (i) BuMgBr, $Fe(acac)_3$, NMP/THF 10:1, rt.

halogen–metal exchange and subsequent quenching with CO_2 at a low temperature. The tetrahydropyrimidine compound **25** was obtained by catalytic hydrogenation over a Rh/C catalyst.

2.2. Pharmacology

The binding affinities of the compounds at native $GABA_A$Rs were measured by displacement of [^{3}H]muscimol in rat membrane

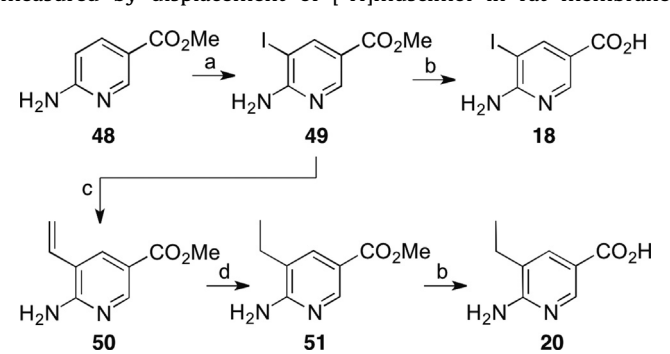

Scheme 4. Reagents and conditions; (a) I_2, Ag_2SO_4, EtOH, (b) Conc. HCl, reflux, (c) CH_2CHBF_3K, $PdCl_2(PPh_3)_2$, K_2CO_3, toluene/H_2O 10:1, 100 °C (d) H_2, Pd/C, THF, rt.

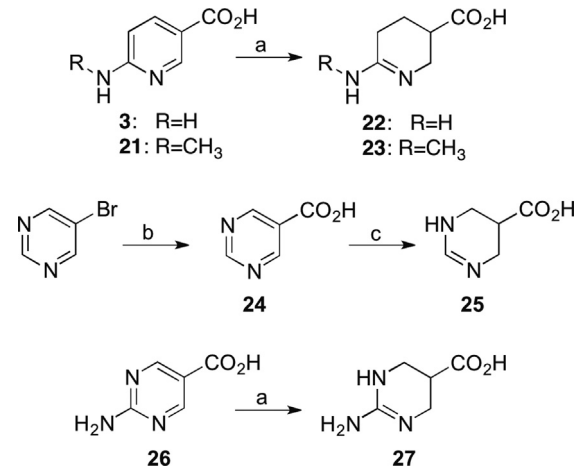

Scheme 5. Reagents and conditions; (a) H_2, PtO_2, conc. HCl, H_2O, rt, (b) nBuLi, THF, EtOH, −110 °C then dry ice, Et_2O, −78 °C to rt, (c) H_2, Rh/C, H_2O.

preparations. Functional characterization of selected compounds was carried out at the human $\alpha_1\beta_2\gamma_{2S}$ and ρ_1 $GABA_A$Rs transiently expressed in tsA201 cells using the FLIPR™ Membrane Potential Blue Assay, performed as described previously [22].

The pharmacological data for the 2-aminopyridine series (**1**–**8**) are given in Table 1 together with data for reference compounds GABA, isoguvacine, and isonipecotic acid. A distinct preference for the positioning of the carboxylic acid or acetic acid moieties in the 4- and 5-positions (R^3 and R^2 in Table 1) is evident, as analogues **3**–**6** display binding affinity in the low micromolar range while 3- and 6-substituted analogues (**1**,**2**,**7**,**8**) are inactive. The parent compounds, isonicotinic acid, nicotinic acid and 3- and 4-aminobenzoic acid (not shown) were devoid of affinity at $GABA_A$R, highlighting importance of the amidine group and not its individual aniline and/or pyridine components.

Table 1
Pharmacological data for reference compounds GABA, isoguvacine, and isonipecotic acid, and **1**–**8**.[a]

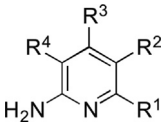

Entry	R^1	R^2	R^3	R^4	[^{3}H]muscimol binding K_i (μM)[b] [pK_i ± SEM]
GABA					0.033[c]
Isoguvacine					0.055 [7.26 ± 0.06]
Isonipecotic acid					0.51 [6.30 ± 0.04]
1	CO_2H	H	H	H	>100
2	CH_2CO_2H	H	H	H	>100
3	H	CO_2H	H	H	4.4 [5.39 ± 0.09]
4	H	CH_2CO_2H	H	H	90 [4.05 ± 0.06]
5	H	H	CO_2H	H	19 [4.72 ± 0.02]
6	H	H	CH_2CO_2H	H	73 [4.14 ± 0.02]
7	H	H	H	CO_2H	>100
8	H	H	H	CH_2CO_2H	>100

[a] $GABA_A$ receptor binding affinities at rat synaptic membranes.
[b] IC_{50} values were calculated from inhibition curves and converted to K_i values. Data are given as the mean [mean pK_i ± SEM] of three to four independent experiments.
[c] From Ref [58].

Compound **3** displayed the highest binding affinity of the compounds initially tested and was chosen as the main scaffold for further SAR studies. Introduction of a range of substituents in the available positions of the pyridine ring was performed (Table 2). Unbranched alkyl groups as substituents in the 2-position of **3** such as methyl, ethyl and butyl are tolerated, compounds **9**–**11** exhibiting binding affinities for the $GABA_AR$ sites comparable to or slightly higher than that of **3**. However, substituents such as phenyl and chloro (**12**,**13**) were detrimental for $GABA_AR$ binding. A similar SAR was observed for the corresponding 4-substituted analogues (**14**–**17**). In sharp contrast to this, the 5-position of **3** did not tolerate any substitutions; iodide, methyl and ethyl substituted compounds **18**–**20** displayed no significant binding at concentrations up to 100 μM.

Conversion of **3** to the tetrahydropyridine compound **22** lead to a 100-fold increase in binding affinity, thus displaying a binding affinity similar to those of GABA and isoguvacine (Table 3). Analogously to compound **3**, introduction of a methyl substituent in the amino nitrogen in **22** given rise to compound **23** lead to a significant decrease in binding affinity.

The pyrimidine and 2-aminopyrimidine carboxylic acids **24** and **26** were devoid of binding affinity for the $GABA_AR$ at concentrations up to 100 μM. However, analogously to **3** and the corresponding tetrahydropyridine analogue **22**, their non-aromatic counterparts **25** and **27** displayed binding affinities in the high nanomolar to low micromolar range.

With respect to the functional properties of the analogous, **3** and the 2-methylated analogue **9** were found to be weak agonists at $\alpha_1\beta_2\gamma_{2S}$ and ρ_1 $GABA_ARs$ transiently expressed in tsA201 cells using the FMP assay (Table 4). The agonist activity decreased upon introduction of larger substituents leading to compounds that were inactive at concentrations up to 1000 μM. Interestingly, the non-

Table 3
Pharmacological data for **3**, **22**–**27**.[a]

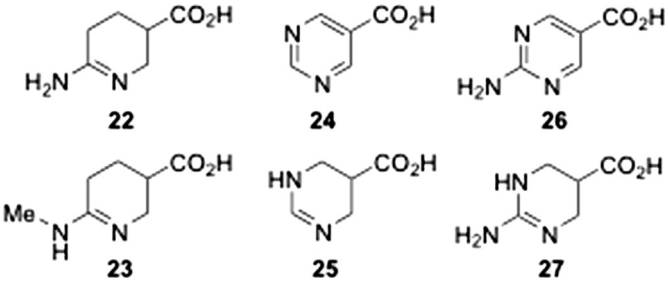

Entry	[^{3}H]muscimol binding K_i (μM)[b] [pK_i ± SEM]	$\alpha_1\beta_2\gamma_{2S}$ EC_{50} (μM) [pEC_{50} ± SEM]	pK_aH[c]
3	4.4 [5.39 ± 0.09]	nd	6.2
22	0.044 [7.36 ± 0.01]	2.6 [5.58 ± 0.09]	12.4
23	49 [4.32 ± 0.06]	>1000 [<3.0]	nd
24	>100	nd	~1.4
25	5.3 [5.29 ± 0.08]	Agonist, R_{max} 25 ± 4.9 at 1 mM	12.2
26	>100	nd	1.9
27	0.54 [6.27 ± 0.05]	14 [4.85 ± 0.08]	12.7

[a] $GABA_A$ receptor binding affinities at rat synaptic membranes and functional characterization at the human $\alpha_1\beta_2\gamma_{2S}$ $GABA_A$ receptors transiently expressed in tsA201 cells using the FLIPR™ Membrane Potential Blue assay.
[b] IC_{50} values were calculated from inhibition curves and converted to K_i values. Data are given as the mean [mean pK_i ± SEM] of three to four independent experiments.
[c] pK_aH determination by diode array detector or potentiometric detection [49]. nd: not determined.

Table 2
Pharmacological data for reference compounds GABA, muscimol, isoguvacine, and isonipecotic acid, and **3**, **9**–**21**.[a]

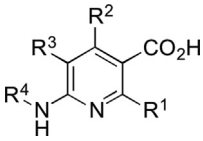

Entry	R^1	R^2	R^3	R^4	[^{3}H]muscimol binding K_i (μM)[b] [pK_i ± SEM]	$\alpha_1\beta_2\gamma_{2S}$ EC_{50} (μM) [pEC_{50} ± SEM]	ρ_1 EC_{50} (μM) [pEC_{50} ± SEM]
GABA					0.033[c]	1.8 [5.75 ± 0.05]	0.27 [6.57 ± 0.02]
Muscimol					0.006[c]	0.54 [6.27 ± 0.06]	0.70 [6.16 ± 0.08]
Isoguvacine					0.055 [7.26 ± 0.06]	11 [4.95 ± 0.09]	39 [4.41 ± 0.08]
Isonipecotic acid					0.51 [6.30 ± 0.04]	Agonist R_{max} 66 ± 5.9 at 1 mM	Weak agonist[c]
3	H	H	H	H	4.4 [5.39 ± 0.09]	>300 [<3.5]	Weak agonist[c]
9	Me	H	H	H	1.4 [5.87 ± 0.06]	Weak agonist[c]	Weak agonist[c]
10	Et	H	H	H	2.1 [5.68 ± 0.02]	>1000 [<3.0]	>1000 [<3.0]
11	Bu	H	H	H	7.1 [5.15 ± 0.03]	>1000 [<3.0]	>1000 [<3.0]
12	Ph	H	H	H	>100	nd	nd
13	Cl	H	H	H	>100	nd	nd
14	H	Me	H	H	3.6 [5.44 ± 0.00]	>1000 [<3.0]	Weak agonist[d]
15	H	Et	H	H	9.3 [5.03 ± 0.03]	>1000 [<3.0]	>1000 [<3.0]
16	H	Bu	H	H	24 [4.63 ± 0.07]	>1000 [<3.0]	>1000 [<3.0]
17	H	Ph	H	H	>100	nd	nd
18	H	H	I	H	>100	nd	nd
19	H	H	Me	H	>100	nd	nd
20	H	H	Et	H	>100	nd	nd
21	H	H	H	Me	>100	nd	nd

[a] $GABA_A$ receptor binding affinities at rat synaptic membranes and functional characterization at the human $\alpha_1\beta_2\gamma_{2S}$ and ρ_1 $GABA_A$ receptors transiently expressed in tsA201 cells using the FLIPR™ Membrane Potential Blue assay.
[b] IC_{50} values were calculated from inhibition curves and converted to K_i values. Data are given as the mean [mean pK_i ± SEM] of three to four independent experiments.
[c] From Ref [58].
[d] Weak agonist response at 1 mM. nd: not determined.

Table 4
Functional characteristics of GABA, muscimol, isoguvacine, isonipecotic acid, **22** and **27** at the human $\alpha_1\beta_2\gamma_{2S}$, $\alpha_2\beta_2\gamma_{2S}$, $\alpha_3\beta_2\gamma_{2S}$, $\alpha_5\beta_2\gamma_{2S}$ and ρ_1 $GABA_AR$ subtypes transiently expressed in tsA201 cells in the FLIPR™ Membrane Potential Blue assay.

Entry	$\alpha_1\beta_2\gamma_{2S}$ EC_{50} (μM) [pEC_{50} ± SEM] R_{max} ± SEM[a] (%)	$\alpha_2\beta_2\gamma_{2S}$ EC_{50} (μM) [pEC_{50} ± SEM] R_{max} ± SEM (%)	$\alpha_3\beta_2\gamma_{2S}$ EC_{50} (μM) [pEC_{50} ± SEM] R_{max} ± SEM (%)	$\alpha_5\beta_2\gamma_{2S}$ EC_{50} (μM) [pEC_{50} ± SEM] R_{max} ± SEM (%)	ρ_1 EC_{50} (μM) [pEC_{50} ± SEM] R_{max} ± SEM (%)
GABA	1.8 [5.75 ± 0.05] 100	0.65 [6.18 ± 0.06] 100	0.92 [6.04 ± 0.04] 100	0.11 [6.97 ± 0.12] 100	0.27 [6.57 ± 0.02] 100
Muscimol	0.54 [6.27 ± 0.06] 93 ± 8.9	0.41 [6.39 ± 0.14] 99 ± 10	0.21 [6.67 ± 0.10] 97 ± 3.5	0.054 [7.27 ± 0.11] 114 ± 11	0.70 [6.16 ± 0.08] 98 ± 9.1
Isoguvacine	13 [4.89 ± 0.06] 85 ± 7.6	4.5 [5.35 ± 0.11] 95 ± 4.3	5.6 [5.25 ± 0.10] 91 ± 4.7	0.78 [6.10 ± 0.09] 101 ± 8.4	3.1 [5.51 ± 0.06] 85 ± 13
Isonipecotic acid	Agonist[b] R_{max} 66 ± 5.9 at 1 mM	24 [4.62 ± 0.04] 85 ± 6.7	17 [4.77 ± 0.09] 85 ± 3.5	2.8 [5.54 ± 0.06] 115 ± 5.9	Weak agonist[b]
22	2.6 [5.58 ± 0.09] 69 ± 5.1	0.82 [6.08 ± 0.12] 101 ± 7.4	1.1 [5.98 ± 0.07] 93 ± 4.2	0.092 [7.04 ± 0.09] 100 ± 4.7	2.3 [5.91 ± 0.05] 64 ± 5.3
27	14 [4.85 ± 0.08] 33 ± 2.5	9.4 [5.03 ± 0.06] 91 ± 6.1	19 [4.71 ± 0.10] 85 ± 4.5	2.1 [5.68 ± 0.07] 113 ± 9.4	8.1 [5.80 ± 0.06] 55 ± 4.9

[a] The R_{max} values are given as percentage of R_{max} of GABA.
[b] Weak agonist response at 1 mM.

aromatic analogue **22** was shown to be equipotent with GABA and isoguvacine as an agonist at the $\alpha_1\beta_2\gamma_{2S}$ $GABA_ARs$.

A subset of compounds was subjected to a broader functional profiling at the human $\alpha_1\beta_2\gamma_{2S}$, $\alpha_2\beta_2\gamma_{2S}$, $\alpha_3\beta_2\gamma_{2S}$, $\alpha_5\beta_2\gamma_{2S}$, and ρ_1 $GABA_AR$ subtypes in the FMP assay. Analogously to the standard agonists GABA, muscimol and isoguvacine, **22** and **27** displayed agonist activities at all tested $GABA_AR$ subtypes with only minor variations among the different subtypes (Table 4). A tendency to lower EC_{50} values at the extrasynaptic $\alpha_5\beta_2\gamma_{2S}$ subtype is normally seen for $GABA_A$ agonists and was also evident in this study. Interestingly, compounds **22** and **27** showed a partial agonist profile at the $\alpha_1\beta_2\gamma_{2S}$ and ρ_1 $GABA_ARs$ in the assay, displaying maximal responses in the range of 33–69% of the maximal response elicited by GABA at the two receptors. In general compounds **22** and **27** were less efficacious than the standard agonists included in this study, whereas they were full agonists (100–113% of R_{max} of GABA) at the $\alpha_5\beta_2\gamma_{2S}$. It is important to stress that whereas we have found the FMP assay to be very predictive when it comes to the rank order of agonist potencies, the efficacies displayed by $GABA_A$ and nAChR agonists in the assay have differed substantially from those obtained in at the respective receptors expressed in the *Xenopus* oocyte expression system. Thus, we will refrain from drawing any solid conclusions about the apparent different agonist efficacies displayed by **22** based on the FMP data in this study.

2.3. Computational modelling

To aid in compound design, the surface of the GABA binding site in the $\alpha_1\beta_2\gamma_2$ $GABA_AR$ homology model [20] was mapped using the program GRID (C3 probe) (Fig. 2).

GRID calculations revealed a hydrophobic cavity below the agonist binding site (extending towards the membrane) and further, slight alterations of rotameric states of α_1Leu117 and α_1Arg119 exposed an additional cavity above the agonist binding site (facing away from the membrane) which is in agreement with similar cavities observed in an antagonist bound model (Fig. 2) [21].

In the homology model, GABA and muscimol were predicted to form a salt bridge with α_1Arg66 and further accepts hydrogen bonds from the two threonines, α_1Thr129 and β_2Thr202 via the carboxylic acid moiety and further to form a salt bridge and hydrogen bonds with residues β_2Glu155 and β_2Ser156 as well as a π–cation interaction with β_2Tyr205 via the protonated amine. [20] Using an induced fit docking protocol, a similar binding mode was obtained for **3**, with hydrogen bond interactions from the protonated amidine group to β_2Glu155 and the backbone carbonyls of β_2Ser156 and β_2Tyr157. At the carboxylic acid end of the molecule, an alternative orientation of the carboxylic acid moiety and Arg66 was observed (Fig. 3A). In this binding pose, the 2- and 4-positions of compound **3** aligned with the observed upper and lower cavities, respectively (Fig. 2). This orientation precluded interaction with Thr129. An alternative binding pose fulfilling all interactions to residues implied in GABA binding was excluded due to high internal energy (see Supporting Information). Analogues of **3** with substituents in the 2- and 4-positions (**9**–**12** and **14**–**16**) were docked and found to align well with the docked pose of **3** and with substituents placed in the observed cavities as illustrated in Fig. 3B and C (For docking scores please refer to Supporting Information).

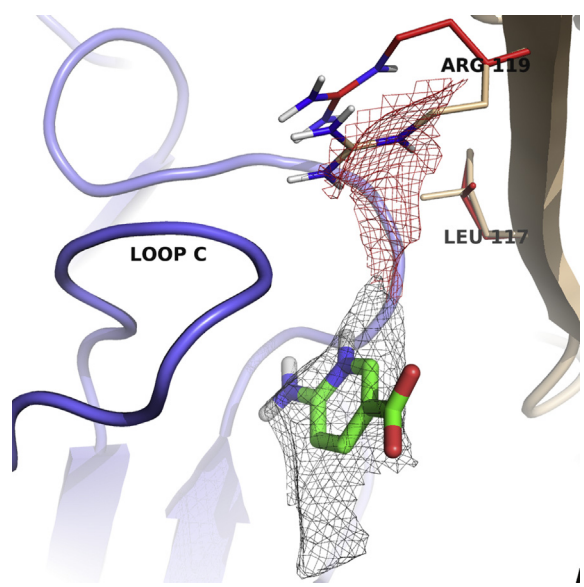

Fig. 2. Outline of the GABA agonist binding site. Molecular interaction field calculations performed with the program GRID using a methyl (C3) probe (grey mesh, −1 kcal/mol) reveals an extension to the pocket protruding downwards towards the membrane. In the upward direction (away from the membrane) the site is capped by α1Leu117 and α1Arg119 (sticks, wheat coloured carbons). Alteration of the rotameric state of these residues (sticks, red carbons) reveals an extension to the pocket (red mesh, −1 kcal/mol). The binding pose for **3** (obtained by induced fit docking as described for ligand docking in the experimental section) is superimposed on the model to illustrate the position of the cavities relative to the template molecule. (For interpretation of the references to colour in this figure legend, the reader is referred to the web version of this article.)

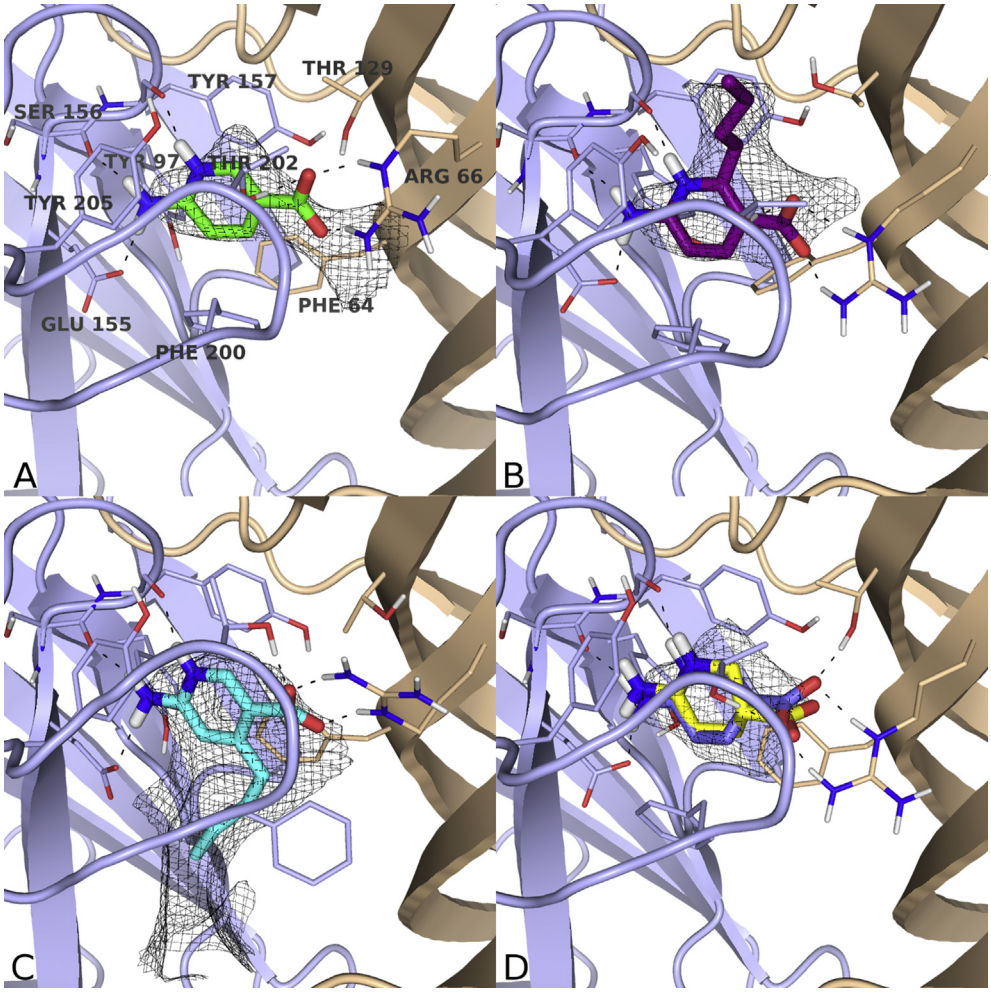

Fig. 3. Predicted binding modes for compounds (A) **3** (green carbons), (B) **11** (purple carbons), (C) **16** (cyan carbons) and (D) **22** (yellow and slate coloured carbons, for the (*R*)- and (*S*) enantiomer respectively). Grey mesh indicates the shape of the pocket determined by the steric GRID methyl probe visualized at energy level of −1 kcal/mol. (For interpretation of the references to colour in this figure legend, the reader is referred to the web version of this article.)

The docked pose of the tetrahydropyridine analogue **22** was observed to fulfil all interactions seen for GABA without resulting in a high internal energy as it was observed for **3** (Fig. 3D and Supporting Information).

3. Discussion and conclusion

Bioisosteric replacement of the carboxylic acid group of GABA has been widely explored [6,31,32], while the amino group at the other end of the molecule has received much less attention. It has been reported that alkylation of the amino group in GABA and muscimol leads to almost complete loss of affinity for the GABA receptor site [33]. However, if a secondary amine function is incorporated in a cyclic structure, as in isoguvacine [8] and THIP [9], $GABA_AR$ binding affinity is retained. Incorporation of the amino group in an amidine system, such as that found for guanidinoacetic acid [34] and guanidinopropionic acid [35] or even in cyclic amidines like imidazole acetic acid and amino-2-thiazolin-4-ylacetic acid [36], restores to some degree the affinity for the GABA receptor site. Finally, a series of highly potent $GABA_AR$ antagonists with the amine being part of an aminopyridazine ring system, including the standard antagonist gabazine, have been reported [37].

In the present study we have introduced the 2-aminopyridine and analogous amidine/guanidine ring systems as novel amine bioisosteres within the $GABA_AR$ area. In addition to the bioisosteric potential, the 2-aminopyridine functionality forms a structurally restricted scaffold suitable for probing the $GABA_AR$ binding site aiming for subtype selectivity.

The bioisosteric relationship was validated and the optimal position of the carboxyl acid group on the 2-aminopyridine ring was first investigated to focus the following SAR studies. A clear preference for a carboxyl group in the 4- or 5-positions of the 2-aminopyridine ring system was observed. Compounds **3** and **5** displayed affinities in the low micromolar range (K_i 4.4 and 19 μM) suggesting that these compounds were characterized by optimal distances between the basic and acidic functionalities for the 2-aminopyridine scaffold.

Based on molecular interaction fields and docking, **3** seemed ideal as a template to probing the two pockets observed in the homology model by substitutions in the 4-position or 2-position of the 6-aminopyridine ring system.

In contrast to the limited substitution generally tolerated for $GABA_A$ agonists, introduction of methyl, ethyl and even a butyl group in the 2- or 4-position of the 6-aminopyridine ring of **3** (**9**–**11**, **14**–**16**) was allowed and did not change binding affinity significantly. Thereby, the identified binding mode of **3**, **9**–**11** and **14**–**16** was supported. In contrast, introduction of methyl and ethyl substituents in the 5-position of **3** leads to loss of affinity. We have

previously reported on a series of analogues of the low efficacy $GABA_AR$ agonist 4-PIOL, where a similar SAR pattern was observed. Introducing unbranched alkyl substituents into the 4-position of the 3-isoxazolol ring of 4-PIOL, elicited a similar response as seen for the 2- and 4-substituted variants of **3**. Further probing of the binding pocket by structurally similar 3-hydroxyisothiazole and 1-hydroxypyrazole scaffolds also reflected these findings [38]. The combined SAR data from these studies verify the performed GRID calculations that imply spacious cavities in the $GABA_AR$ binding site pocket above and below the central cavity where the core scaffolds binds.

Incorporating the amino group of GABA in a pyrimidine or pyrimidin-2-amine ring system, **24** and **26**, led to compounds devoid of affinity. Though mimicking the electron distribution in the guanidinic/amidinic system, the significantly lowered pK_{aH} values (pK_{aH} 1.4–1.9), with an increasing uncharged fraction of compound at physiological pH, most likely result in loss of affinity.

In general, a significant increase in binding affinities was observed for the tetrahydro analogues, **22**, **25**, **27**, of 2-aminopyridine, pyrimidine and 2-aminopyrimidine compared to their parent compounds, **3**, **24** and **26**. For the 2-aminotetrahydropyridine analogue of **3** (**22**), a 100-fold increase in affinity was observed. At least two different effects could be held accountable for this: 1) Increased conformational flexibility of **22** allowing it to form interactions identical to those of GABA as opposed to **3** which has to assume a high energy conformation to do the same (Supporting Information). 2) Significant changes in pK_{aH} values for the basic groups (Table 3). The more basic amidine group in **22** is to a larger extent protonated and may form stronger interactions in the binding pocket relative to **3.**

To challenge the importance of the basic center, analogues to **3** containing only one nitrogen atom in the basic center; 3- and 4-pyridine and 3- and 4-anilin, were included in the study. They showed no affinity for the $GABA_ARs$ in agreement with the need for a positive ionisable group [39,40]. The slightly lower pK_{aH} values of the pyridine and aniline groups compared to the 2-aminopyridine group likely influence the extent of protonation thereby affecting the strength of interactions involving the basic center. Further, introduction of a methyl group in the external amino group in **3** affording **21** and in the corresponding tetrahydro analogue **22** affording **23** abolished $GABA_AR$ affinity. A similar detrimental effect has been reported for muscimol and the secondary amine analogues isoguvacine and THIP [8,41,42]. These observations suggest that ligands for the GABA receptors are sensitive to steric hindrance in proximity of the cationic moiety of the molecule, and that the primary or secondary structure of the amino group is of minor importance.

Despite the obvious need for subtype selective GABA ligands only few orthosteric $GABA_AR$ agonists have been systematically characterized on different $GABA_AR$ subtypes [43,44]. In general, only small differences in binding affinities and agonist activity were observed reflecting the high degree of similarity between the individual $GABA_AR$ binding sites. However, THIP and allosteric modulators for the benzodiazepine binding site [45] show that functional selectivity can be obtained for both orthosteric ligands and modulators at some receptor subtypes in spite of a lack of binding selectivity.

In the present study, $\alpha_5\beta_2\gamma_{2S}$ subtype preference was observed for **22** based on potency, which is in line with observations on $GABA_AR$ agonists in general. The $\alpha_5\beta_2\gamma_{2S}$ $GABA_AR$ subtype is located largely at extrasynaptic sites, primarily in hippocampus, where they are subject to activation of low ambient GABA concentration mediating tonic inhibition distinct from the transient activation of synaptic $GABA_ARs$ leading to classical inhibitory postsynaptic phasic currents [46]. The tonic inhibition mediated by extrasynaptic α_5-subunit containing $GABA_ARs$ are proposed to be involved in learning and memory [47]. Interestingly, **22** as well as **27** were shown to be full agonists at the extrasynaptically $\alpha_5\beta_2\gamma_{2S}$ subtype and less efficacious at the synaptically localized $GABA_AR$ subtypes ($\alpha_1\beta_2\gamma_{2S}$, $\alpha_2\beta_2\gamma_{2S}$, $\alpha_3\beta_2\gamma_{2S}$, and ρ_1). This observed tendency towards functional selectivity for the $\alpha_5\beta_2\gamma_{2S}$ $GABA_AR$ subtype is also seen for isoguvacine and especially isonipecotic acid in this study. Considering the coarse nature of the FMP assay these findings have to be confirmed by electrophysiological recordings at $GABA_ARs$ expressed in e.g. *Xenopus* oocytes.

3.1. Conclusion

The study identified the 2-aminopyridine and 2-aminotetrahydropyridine/pyrimidine scaffolds as bioisosteres for the amino group in GABA at $GABA_A$ receptors. A series of 2-aminopyridine/pyrimidine carboxylic acid (**1**–**21**, **24**, **26**) and corresponding tetrahydro analogues (**22**, **23**, **25**, **27**) have been synthesized and characterized pharmacologically at $GABA_ARs$. The 2-aminopyridine analogue 6-aminonicotinic acid (**3**) was shown to be a weak agonist, and SAR studies showed that substitutions in the 2- and 4-position were tolerated. The tetrahydro analogues (**22**, **25**, **27**) were shown to be moderate to potent agonists (K_i of 0.044–5.4 μM). Cavities surrounding the core of the GABA binding pocket were predicted by molecular interaction field calculations and docking studies, and were confirmed by affinities of substituted analogues of **3**. This is in line with previous SAR studies of the significantly larger 4-PIOL analogues but has not previously been reported in relation to agonists. The bioisosteric properties of the novel scaffolds are supported by a common binding mode and similar interactions for the tetrahydro analogues of **3** and GABA itself, which is in agreement with the observed agonist profile. These findings have prompted us to further elucidate the structural features of this class of GABA analogues in regard to the identified cavities and the observed agonist profile, subtype selectivity and activity at other GABA related targets. New possibilities have been revealed for ligand design for the orthosteric binding site in general paving the way for diversity in both agonist structure and pharmacological profile.

4. Experimental section

4.1. Chemistry

4.1.1. General procedures

Reagents and solvents were obtained from commercial suppliers and used without further purification. Anhydrous CH_2Cl_2, DMF and THF were obtained by using a solvent purification system, and other anhydrous solvents were obtained by storage over 4 Å molecular sieves. All reactions involving air- and/or moisture sensitive reagents were performed under a nitrogen atmosphere using syringe-septum cap techniques and/or with flame-dried glassware. Analytical thin-layer chromatography (TLC) was carried out using Merck silica gel 60 F254 plates and the compounds were visualized with UV light (254 nm), ninhydrin or $KMnO_4$ spraying agents. NMR spectra were recorded on a 300 MHz Varian Mercury Plus spectrometer, a 300 MHz Varian Gemini 2000 spectrometer or a 400 MHz Bruker Avance spectrometer. Dry column vacuum chromatography (DCVC) [48] was performed using Fischer Scientific silica gel 60 (20–45 μm). Flash chromatography (FC) was performed using Merck silica gel 60 (40–63 μm). Reverse phase FC (RP-FC) was performed using Merck LiChroprep RP-18 (40–63 μm). Analytical HPLC (anal. HPLC) was performed on a Merck-Hitachi HPLC system consisting of an L-7100 pump, an L-7200 autosampler, and an L-7400 UV detector (254 nm), using an X-Terra column

(4.6 × 150 mm) eluted at a flow rate of 0.8 mL/min. A linear gradient elution was performed with eluent A (H_2O-TFA 100:0.1) containing 0% of solvent B (MeCN–H_2O–TFA, 90:10:0.01) rising to 100% of B during 25 min. Data were acquired and processed using the EZChrom Elite Software version 3.1.7 by Hitachi. All microwave reactions were carried out in a glass reactor using a Biotage Initiator instrument. Melting points were determined by OptiMelt from Stanford Research Systems in open capillary tubes and are uncorrected. Elemental analysis was performed by Mr. J. Theiner, Department of Physical Chemistry, University of Vienna, Austria and are within ±0.4% of the calculated values unless otherwise stated.

4.1.2. General procedure for hydrolysis (**9**–**12**, **14**–**20**)

The protected compounds (**33**–**35**, **39**–**41**, **51**) were dissolved in 6 M or conc. HCl and heated at reflux using conventional heating or microwave irradiation for 12 h to 4 days followed by evaporation under vacuum.

4.1.2.1. 6-Amino-2-methylnicotinic acid hydrochloride (**9**).

Hydrolysis according to the general procedure using **33** (200 mg, 1.50 mmol), 6 M HCl, conventional heating, 24 h. Recrystallization from EtOH/Et_2O afforded the product as brown solid (218 mg, 77%). An analytical amount was washed with hot MeCN and used for characterization and in pharmacological tests. ^{1}H NMR (D_2O): δ 8.31 (d, J = 9.4 Hz, 1H), 6.91 (d, J = 9.4 Hz, 1H), 2.77 (s, 3H). ^{13}C NMR (D_2O): δ 167.8, 154.9, 152.0, 145.0, 115.1, 110.3, 18.8. Anal. ($C_7H_8N_2O_2 \cdot 1.5HCl$) C, H, N.

4.1.2.2. 6-Amino-2-ethylnicotinic acid hydrochloride (**10**).

Hydrolysis according to the general procedure using **39** (124 mg, 0.84 mmol), conc. HCl, conventional heating, 3 days. Purification by RP-DCVC (0.1% TFA in H_2O) followed by evaporation from conc. HCl, and recrystallization from EtOH afforded the product as white crystals (16 mg, 10%). mp 254.4–255.7 °C. ^{1}H NMR (D_2O) δ 8.17 (m, 1H), 6.77 (m, 1H), 3.04 (m, 2H), 1.20 (m, 3H). ^{13}C NMR (D_2O) δ 167.7, 156.8, 155.1, 145.2, 114.4, 110.4, 25.5, 13.0. Anal. ($C_8H_{10}N_2O_2 \cdot 1.1HCl$) C, H, N.

4.1.2.3. 6-Amino-2-butylnicotinic acid hydrochloride (**11**).

Hydrolysis according to the general procedure using **40** (225 mg, 1.28 mmol), conc. HCl, conventional heating, 4 days. Purification by RP-DCVC (0.1% TFA/MeCN 100:0 to 95:5) followed by evaporation from conc. HCl, and recrystallization from EtOH afforded the product as off-white crystals (18 mg, 6%). mp 212.8–215 °C. ^{1}H NMR (D_2O) δ 8.11–8.22 (m, 1H), 6.86–6.66 (m, 1H), 3.09–2.95 (m, 2H), 1.65–1.49 (m, 2H), 1.39–1.23 (m, 2H), 0.89–0.77 (m, 3H). ^{13}C NMR (D_2O) δ 167.8, 155.7, 155.1, 145.1, 114.9, 110.3, 31.6, 31.2, 21.9, 12.9. Anal. ($C_{10}H_{14}N_2O_2 \cdot 1.1HCl$) C, H, N.

4.1.2.4. 6-Amino-2-phenylnicotinic acid hydrochloride (**12**).

Hydrolysis according to the general procedure using **41** (175 mg, 0.90 mmol), conc. HCl, conventional heating, 4d. Recrystallization from MeOH afforded the product as light brown solid (23 mg, 10%). mp 205.7–207.4 °C. ^{1}H NMR (MeOH-d_4) δ 8.41 (d, J = 9.5 Hz, 1H), 7.54 (m, 5H), 7.05 (d, J = 9.5, 1H). ^{13}C NMR (MeOH-d_4) δ 166.6, 157.1, 152.5, 146.4, 134.3, 131.9, 130.1, 129.7, 117.2. 113.2. Anal. ($C_{12}H_{10}N_2O_2 \cdot 1.3$ HCl) C, H, N.

4.1.2.5. 6-Amino-4-methylnicotinic acid trifluoroacetic acid (**14**).

Hydrolysis according to the general procedure using **34** (482 mg crude), conc. HCl, conventional heating, 24 h. Purification by RP-DCVC followed by recrystallization from H_2O afforded the product as white crystals (163 mg, 23% over 2 steps). ^{1}H NMR (D_2O) δ 8.37 (s, 1H), 6.82 (s, 1H), 2.56 (s, 3H). ^{13}C NMR (D_2O) δ 167.7, 157.2, 154.9, 140.7, 116.3, 114.1, 21.8. Anal. ($C_7H_8N_2O_2 \cdot CF_3COOH$) C, H, N.

4.1.2.6. 6-Amino-4-ethylnicotinic acid hydrochloride (**15**).

Hydrolysis according to the general procedure using **45** (96 mg, 0.65 mmol), conc. HCl, microwave irradiation, 12 h. Recrystallization from MeOH afforded the product as off-white solid (41 mg, 31%). mp (decomp.) >245 °C. ^{1}H NMR (MeOH-d_4) δ 8.44 (d, J = 0.8 Hz, 1H), 6.88 (q, J = 0.8 Hz, 1H), 3.11 (dq, J = 0.75 Hz, J = 7.30, 2H), 1.26 (t, J = 7.3 Hz, 3H). ^{13}C NMR (MeOH-d_4) δ 166.0, 164.6, 156.4, 141.7, 117.6, 113.7, 28.8, 14.3. Anal. ($C_8H_{10}N_2O_2 \cdot HCl$) C, H, N.

4.1.2.7. 6-Amino-4-butylnicotinic acid hydrochloride (**16**).

Hydrolysis according to the general procedure using **46** (83 mg, 0.38 mmol), conc. HCl, microwave irradiation, 12 h. The solvent was decanted, and the precipitate dried under vacuum affording the product as off-white crystals (70 mg, 79%). mp 195.3–198.0 °C. ^{1}H NMR (D_2O) δ 8.36 (s, 1H), 6.85 (s, 1H), 2.96 (m, 2H), 1.54 (m, 2H), 1.35 (sxt, J = 7.3 Hz, 2H), 0.89 (t, J = 7.3 Hz, 3H). ^{13}C NMR (D_2O) δ 167.6, 161.6, 154.0, 139.7, 117.0, 113.2, 33.6, 31.5, 21.9, 13.0. Anal. ($C_{10}H_{14}N_2O_2 \cdot 1.05$ HCl) C, H, N.

4.1.2.8. 6-Amino-4-phenylnicotinic acid hydrochloride (**17**).

Hydrolysis according to the general procedure using **47** (120 mg, 61 mmol), conc. HCl, microwave irradiation, 12 h. Recrystallization from MeOH/Et_2O afforded the product as white solid (20 mg, 7%). mp (decomp.) >207 °C. ^{1}H NMR (MeOH-d_4) δ 7.19 (d, J = 0.8 Hz, 1H), 6.19 (m, 3H), 6.12 (m, 2H), 5.65 (d, J = 0.8 Hz, 1H). ^{13}C NMR (MeOH-d_4) δ 166.4, 159.1, 156.1, 141.1, 138.8, 130.7, 129.5, 129.0, 118.5, 115.6. Anal. HPLC purity 95% (254 nm).

4.1.2.9. 6-Amino-5-iodonicotinic acid hydrochloride (**18**) [28].

Hydrolysis according to the general procedure using **49** (60 mg, 0.22 mmol), conc. HCl, conventional heating, 24 h. Recrystallization from MeOH/Et_2O afforded the product as white crystals (59 mg, 91%). mp. 280–284 °C. ^{1}H NMR (CD_3OD) δ 8.82 (d, J = 1.8 Hz, 1H), 8.50 (d, J = 1.8 Hz, 1H). ^{13}C NMR (CD_3OD) δ 163.4, 155.9, 153.2, 139.7, 118.1, 79.3. Anal. ($C_6H_5IN_2O_2 \cdot 0.8HCl$): C, H, N.

4.1.2.10. 6-Amino-5-methylnicotinic acid hydrochloride (**19**).

Hydrolysis according to the general procedure using **35** (200 mg, 1.50 mmol), 6 M HCl, conventional heating, 24 h. Recrystallization from EtOH/Et_2O afforded the product as grey solid (233 mg, 83%). ^{1}H NMR (D_2O) δ 8.31 (s, 1H), 8.09 (s, 1H), 2.21 (s, 3H). ^{13}C NMR (D_2O) δ 166.9, 154.9, 141.9, 137.0, 123.1, 166.6, 16.1. Anal. HPLC purity 99% (254 nm).

4.1.2.11. 6-Amino-5-ethylnicotinic acid hydrochloride (**20**).

Hydrolysis according to the general procedure using **51** (70 mg, 0.39 mmol), conc. HCl, conventional heating, 24 h. Recrystallization from EtOH/Et_2O afforded the product as white solid (71 mg, 91%). mp. 265–268 °C. ^{1}H NMR ($CDCl_3$) δ 8.59 (d, J = 2.1 Hz, 1H), 7.85 (d, J = 2.1 Hz, 1H), 5.30 (b s, 2H), 2.45 (q, J = 7.5 Hz, 2H), 1.28 (t, J = 7.5 Hz, 3H). ^{13}C NMR ($CDCl_3$) δ 167.0, 160.1, 149.0, 136.4, 121.3, 116.9, 52.1, 23.7, 12.21. Anal. ($C_8H_{10}N_2O_2 \cdot 1.1$ HCl) C, H, N.

4.1.3. 2-(2-Aminopyridin-4-yl)acetic acid hydrochloride (**6**)

Aqueous NaOH (1 M, 1.7 mL) was added to a solution of **29** (0.393 g, 1.4 mmol) in MeOH (8 mL). The reaction mixture was heated to reflux for 20 min. Conc. HCl (0.17 mL) was added to pH 4 followed by evaporation under vacuum. Ion exchange and recrystallisation from isopropanol/water afforded the product as colourless crystals (122 mg, 39%). ^{1}H NMR (300 MHz, D_2O): δ 7.64 (1H, d, J = 6.3 Hz), 6.82 (1H, s), 6.75 (1H, d, J = 6.3 Hz), 3.65 (2H, s). ^{13}C NMR

(75 MHz, D_2O): 174.9, 154.0, 153.4, 135.1, 115.1, 114.1, 67.2. Anal. ($C_7H_8N_2 \cdot 0.8$ HCl) C, H, N.

4.1.4. 6-Amino-2-chloronicotinic acid (**13**)

A solution of **37** (200 mg, 0.79 mmol) in anhydrous THF/Et_2O (1:1, 12.5 mL) was cooled to −110 °C on an EtOH/liquid N_2 bath. *n*-BuLi (2.5 M in hexanes, 0.69 mL, 1.73 mmol) was added dropwise and after 15 min, CO_2 (g) was bubbled through the solution for 35 min while the temperature was allowed to rise to −30 °C. H_2O (10 mL) was added, and the phases were separated. The organic phase was extracted with H_2O (4 × 10 mL) and 1 M NaOH (10 mL). The combined aqueous layer was acidified with 6 M HCl till pH 2 and evaporated partly under vacuum until precipitation occurred. The precipitate was isolated by filtration and dried under vacuum affording the product as brown solid (30 mg, 22%). mp (decomp.) >264 °C. ^{1}H NMR (DMSO-d_6) δ 12.57 (b s, 1H), 7.88 (d, J = 8.5 Hz, 1H), 7.05 (b s, 2H), 6.39 (d, J = 8.5 Hz, 1H). ^{13}C NMR (DMSO-d_6) δ 165.3, 161.0, 149.4, 141.8, 111.9, 106.0. Anal. ($C_6H_5Cl\ N_2O_2$) C, H, N.

4.1.5. 6-(Methylamino)nicotinic acid hydrochloride (**21**)

A solution of 6-chloronicotinic acid (1.00 g, 6.35 mmol) in pyridine (2.0 mL) and methylamine (40% aq. solution, 2.7 mL, 32.0 mmol) was heated using microwave irradiation at 150 °C for 12 h. H_2O (4 mL) was added, and 1 M HCl was added until pH ~ 3, then a few drops of 5 M NaOH was added, and precipitation occurred. The mixture was stored for 3 days at 5 °C, and the precipitate was collected by filtration. The precipitate was washed with cold H_2O and dried under vacuum affording the product as white solid (307 mg, 32%). mp 253.2–254.8 °C. ^{1}H NMR (DMSO-d_6) δ 12.35 (b s, 1H), 8.55 (dd, J = 2.3 Hz, J = 0.5 Hz, 1H), 7.80 (dd, J = 8.8 Hz, J = 2.3 Hz, 1H), 7.32 (d, J = 4.0, 1H), 6.47 (dd, J = 8.8, J = 0.5 Hz, 1H), 2.82 (d, J = 4.0 Hz, 3H). ^{13}C NMR (DMSO-d_6) δ 166.8, 161.3, 150.8, 150.6, 137.3, 113.8, 27.8. Anal. ($C_7H_8N_2O_2 \cdot 0.05$HCl) C, H, N.

4.1.6. 2-Amino-3,4,5,6-tetrahydropyridine-5-carboxylic acid hydrochloride (**22**) [29]

3 (100 mg, 0.72 mmol) was dissolved in water (10 mL) and conc. HCl (0.6 mL). PtO_2 (20 mg, 0.08 mmol) was added and the reaction mixture was hydrogenated at rt for 17 h. The mixture was filtered through cotton wool and evaporated under vacuum. Recrystallization from EtOH afforded the product as pale yellow crystals (50 mg, 39%). mp. (decomp) > 200 °C. ^{1}H NMR (D_2O) 3.63 (m, 2H), 3.03 (m, 1H), 2.75 (t, J = 6.7 Hz, 2H), 2.20 (m, 1H), 2.05 (m, 1H). ^{13}C NMR (D_2O) 176.4, 166.1, 41.9, 36.7, 24.1, 20.1. Anal. ($C_6H_{10}N_2O_2 \cdot 1.1$HCl) C, H, N.

4.1.7. 6-(Methylamino)-2,3,4,5-tetrahydropyridine-3-carboxylic acid hydrochloride (**23**)

Prepared as described for **22** using **21** (100 mg, 0.66 mmol), H_2O (6.5 mL), conc. HCl (0.15 mL), and PtO_2 (20 mg, 0.09 mmol) for 3 days. Recrystallization from glacial AcOH/EtOAc afforded the product as white solid (48 mg, 38%). mp 201.5–204.7 °C. ^{1}H NMR (D_2O) δ 3.66 (dd, J = 13.3 Hz, J = 5.5 Hz, 1H), 3.58 (dd, J = 13.3 Hz, J = 7.5 Hz, 1H), 2.99 (m, 1H), 2.85 (s, 3H), 2.68 (t, J = 6.5 Hz, 2H), 2.17 (m, 1H), 2.00 (m, 1H). ^{13}C NMR (D_2O) δ 176.7, 163.6, 42.1, 37.2, 27.5, 24.6, 20.4. Anal. ($C_7H_{12}N_2O_2 \cdot 1.6$HCl) C, H, N.

4.1.8. Pyrimidine-5-carboxylic acid (**24**) [30]

A solution of 5-bromopyrimidine (1.00 g, 6.29 mmol) in dry Et_2O and dry THF (1:1, 60 mL) was cooled to between −105 °C and −110 °C on an EtOH/liquid N_2 bath and stirred for 15 min. *n*BuLi (4.10 mL, 2.3 M, 9.44 mmol), cooled to −78 °C, was added dropwise under stirring at the same temperature, and the mixture was stirred for additional 10 min. Pellets of dry ice was covered with precooled dry Et_2O (50 mL). The reaction mixture was poured into this mixture and allowed to heat to room temperature. The ether was extracted with water (3 × 50 mL) and 1 N NaOH (50 mL), and the combined water phases were acidified with 1 N HCl. The water was reduced to a quarter volume by freezedrying resulting in precipitation of a white solid. The solid was separated by filtration to give 0.564 g (56%) of product as a white solid. mp. (decomp.) >256 °C. ^{1}H NMR (DMSO-d_6) δ 9.39 (s, 1H), 9.21 (s, 2H) 3.34 (br s., 1H). ^{13}C NMR (DMSO-d_6) δ 164.8, 161.1, 157.7, 124.9. Anal. ($C_5H_4N_2O_2 \cdot 0.2$HCl) C, H, N.

4.1.9. 1,4,5,6-Tetrahydropyrimidine-5-carboxylic acid (**25**)

24 (0.250 g, 1.90 mmol) was dissolved in water (25 mL). Rh/C (0.235 g, 5%, 0.114 mmol Rh) was added and the reaction mixture was flushed with H_2 three times. The reaction mixture was stirred under H_2 over night. The mixture was filtered through cotton wool and evaporated to dryness to give the crude product as a white solid (203 mg, 84%). The product was recrystallized from MeOH and Et_2O to give **25** (120 mg; 49%) as white crystals. mp. (decomp.) >294 °C. ^{1}H NMR (D_2O) δ 7.94 (s, 1H), 3.65 (dd, J = 13.3, 4.8 Hz, 2H), 3.52 (dd, J = 13.4, 7.8 Hz, 2H), 2.90 (m, 1H). ^{13}C NMR (D_2O) δ 177.4, 151.1, 40.4, 36.5. Anal. ($C_5H_8N_2O_2 \cdot 0.05$HCl) C, H, N.

4.1.10. 2-Amino-1,4,5,6-tetrahydropyrimidine-5-carboxylic acid hydrochloride (**27**) [29]

2-Aminopyrimidine-5-carboxylic acid (**26**) (0.200 g, 1.44 mmol) was dissolved in water (20 mL) and conc. HCl (1.2 mL). PtO_2 (0.040 g, 0.176 mmol) was added and the reaction mixture was flushed with H_2 three times and stirred under H_2 for 48 h. The mixture was filtered through cotton wool and evaporated to dryness to give the crude product as a white solid (248 mg, 96%). 100 mg crude product was recrystallized from EtOH to give 41 mg (41%) of white crystals. mp. 258.8–260.5 °C. ^{1}H NMR (D_2O) δ 3.60 (m, 4H), 3.17 (quintet, J = 5.3 Hz, 1H). ^{13}C NMR (D_2O) δ 174.9, 153.7, 39.4, 35.5. Anal. ($C_5H_9N_3O_2 \cdot$HCl) C, H, N.

4.1.11. tert-Butyl 4-methylpyridin-2-ylcarbamate (**28**)

4-Methylpyridine-2-amine (10.0 g, 92 mmol) was added to a solution of di-*tert*-butyl dicarbonate (22.2 g, 102 mmol) in *tert*-butanol (600 mL). The reaction mixture was stirred for 10 h at room temperature followed by evaporation under vacuum. Recrystallisation from isopropanol afforded the product as colourless crystals (19.3 g, 88%): ^{1}H NMR (300 MHz, $CDCl_3$): δ 9.04 (1H, b s), 8.14 (1H, d, J = 4.8 Hz), 7.83 (1H, s), 6.77 (1H, d, J = 4.8 Hz), 2.35 (3H, s), 1.54 (9H, s).

4.1.12. Ethyl 2-(2-(tert-butoxycarbonylamino)pyridin-4-yl)acetate (**29**)

A solution of **28** (1.0 g, 4.8 mmol) in THF (10 mL) was added to a solution of LDA (11 mmol) in THF (5 mL) at −70 °C. Stirring was continued for 1 h at −70 °C and 0 °C for 1 h. Diethylcarbonate (567 μL, 4.8 mmol) was added to the reaction mixture and stirring was continued for 1 h at 0 °C. H_2O (60 mL) was added and the reaction mixture was extracted using Et_2O (3 × 100 mL). The combined organic phase was dried and evaporated under vacuum. Purification by FC (petroleum ether/EtOAc 4:1) afforded the product (400 mg, 30%). ^{1}H NMR (300 MHz, $CDCl_3$): δ 8.52 (1H, b s), 8.19 (1H, d, J = 5.1 Hz), 7.94 (1H, s), 6.92 (1H, d, J = 5.1), 4.16 (2H, q, J = 7.2 Hz), 3.62 (2H, s), 1.53 (9H, s), 1.26 (3H, t, 7.2 Hz).

4.1.13. 6-Amino-2-methylniconitrile (**33**)

A mixture of **30** (500 mg, 2.67 mmol), $Zn(CN)_2$ (188 mg, 1.60 mmol), $Pd_2(dba)_3$ (122 mg, 0.13 mmol), and dppf (148 mg, 0.27 mmol) was added degassed DMF/H_2O (99:1, 3.1 mL). The reaction mixture was heated using conventional heating at 120 °C for

24 h. The resulting mixture was cooled to rt, and sat. aq. NH_4Cl/conc. NH_3/H_2O (4:1:4, 10 mL) was added resulting in precipitation. The mixture was cooled to 0 °C and filtered. The precipitate was washed with sat. aq. NH_4Cl/conc. NH_3/H_2O (4:1:4, 10 mL) and H_2O at 5 °C and dried under vacuum affording the product as dark orange solid (279 mg, 78%). mp. 162–164 °C. IR 2211 cm^{-1}. ^1H NMR ($CDCl_3$) δ 7.54 (d, $J = 8.4$ Hz, 1H), 6.33 (d, $J = 8.4$ Hz, 1H), 5.06 (b s, 2H), 2.55 (s, 3H). ^{13}C NMR ($CDCl_3$) δ 162.8, 159.9, 141.5, 118.9, 105.8, 97.6, 23.8.

4.1.14. 6-Amino-4-methylniconitrile (**34**)

Prepared as described for **33** using **31** (500 mg, 2.67 mmol), $Zn(CN)_2$ (190 mg, 1.60 mmol), $Pd_2(dba)_3$ (122 mg, 0.13 mmol), dppf (12 mg, 0.21 mmol), and degassed DMF/H_2O (99:1, 3 mL) affording the crude product as brown solid (482 mg, 136% crude yield). The product was used without further purification for preparation of **34**. ^1H NMR ($CDCl_3$) δ 8.25 (s, 1H), 6.34 (s, 1H), 4.90 (b s, 2H), 2.39 (s, 3H). ^{13}C NMR ($CDCl_3$) δ 160.9, 153.7, 151.6, 117.8, 110.8, 100.4, 20.53.

4.1.15. 6-Amino-5-methylniconitrile (**35**)

Prepared as described for **33** using **32** (500 mg, 2.67 mmol), $Zn(CN)_2$ (188 mg, 1.60 mmol), $Pd_2(dba)_3$ (6 mg, 0.13 mmol), dppf (14 mg, 0.27 mmol), and degassed DMF/H_2O (99:1, 3.1 mL). Precipitation afforded the product as red-brown solid (281 mg, 79%). mp. 184–188 °C. ^1H NMR ($CDCl_3$) δ 8.03 (s, 1H), 7.04 (s, 1H), 4.94 (b s, 2H) 1.94 (s, 3H). ^{13}C NMR ($CDCl_3$) δ 162.1, 148.7, 140.3, 117.5, 113.8, 98.3, 16.5.

4.1.16. 6-Chloro-5-iodopyridin-2-amine (**37**) [24]

36 (1.00 g, 7.78 mmol) was dissolved in DMF (40 mL), the reaction flask was covered with aluminium foil, and NIS (970 mg, 4.28 mmol) was added. The reaction mixture was stirred for 19 h before additional NIS (970 mg, 4.28 mmol) was added, and the reaction mixture was stirred for another 24 h. H_2O (200 mL) was added, and the mixture was extracted with EtOAc (2 × 250 mL). The combined organic layer was washed with H_2O (2 × 200 mL) and brine (200 mL), dried over Na_2SO_4, and evaporated under vacuum. Recrystallization from EtOH followed by recrystallization of the mother liquor afforded the product as orange, needle-shaped crystals (1.45 g, 73%). mp 154.3–155.9. ^1H NMR ($CDCl_3$) δ 7.75 (d, $J = 8.2$ Hz, 1H), 6.22 (d, $J = 8.2$ Hz, 1H). ^{13}C NMR ($CDCl_3$) δ 157.6, 151.6, 149.4, 108.8.

4.1.17. 6-Amino-2-chloronicotinonitrile (**38**)

Prepared as described for **33** using **37** (4.00 g, 15.7 mmol), $Zn(CN)_2$ (1.11 g, 9.43 mmol), dppf (871 mg, 1.57 mmol), $Pd_2(dba)_3$ (720 mg, 0.78 mmol), and degassed DMF/H_2O (99:1, 20 mL). The reaction mixture was heated at 120 °C using microwave irradiation for 1 h. Precipitation afforded the crude product as a dark green solid (3.66 g, 152% crude yield). 200 mg crude product was purified for characterization by DCVC (heptane/EtOAc/Et_3N 100:0:1 to 60:40:1) affording the product as white solid (62 mg). mp (decomp.) >213 °C. ^1H NMR (DMSO-d_6) 7.76 (d, $J = 8.5$ Hz, 1H), 7.52 (s, 2H), 6.44 (d, $J = 8.5$ Hz, 1H). ^{13}C NMR (DMSO-d_6) δ 161.5, 151.5, 142.3, 117.0, 106.9, 93,5.

4.1.18. 6-Amino-2-ethylnicotinonitrile (**39**)

38 (1.00 g crude, max 4.30 mmol), diethylzinc (1.0 M in hexane, 7.81 mmol, 7.8 mL), and $Pd_2(PPh_3)_4$ (150 mg, 0.13 mmol) were added to a microwave vial along with NMP (8 mL). The vial was flushed with N_2, sealed and heated using microwave irradiation at 100 °C for 30 min. The contents of the vial were cooled to rt and washed with sat. aq. $NaHCO_3$ (120 mL), and H_2O (120 mL), dried over Na_2SO_4, and evaporated under vacuum. Purification by FC (heptane/EtOAc 80:20 to 50:50) afforded the product as brown solid (333 mg, 53% over 2 steps). ^1H NMR ($CDCl_3$) δ 7.56 (d, $J = 8.5$ Hz, 1H), 6.34 (d, $J = 8.5$ Hz, 1H), 4.99 (b s, 2H), 2.86 (q, $J = 7.6$ Hz, 2H), 1.31 (t, $J = 7.6$ Hz, 3H). ^{13}C NMR ($CDCl_3$) δ 167.4, 159.8, 141.4, 118.5, 105.7, 96.6, 30.4, 13.5.

4.1.19. 6-Amino-2-butylnicotinonitrile (**40**)

A mixture of NMP (8 mL), I_2 (82.6 mg, 0.33 mmol), and Zn (809 mg, 12.4 mmol) was stirred at rt until the red colour of I_2 disappeared (ca. 4 min). Butyl-1-bromide (0.88 mL, 8.14 mmol) was added and the mixture was stirred at 80 °C for 3 h. The mixture was cooled to rt and **38** (1.00 g crude, max. 4.30 mmol) and $Pd_2(PPh_3)_4$ (150 mg, 0.13 mmol) were added, and the reaction mixture was stirred at rt for 1 h. Sat. aq. NH_4Cl (120 mL) was added, and the mixture was extracted with EtOAc (2 × 120 mL). The combined organic phase was washed with brine (120 mL), dried over Mg_2SO_4, and evaporated under vacuum. Purification by FC (heptane/EtOAc 100:0 to 0:100) afforded the product with small impurities as light yellow solid (225 mg, 29% over 2 steps). ^1H NMR ($CDCl_3$) δ 7.56 (d, $J = 8.5$ Hz, 1H), 6.35 (d, $J = 8.5$ Hz, 1H), 5.00 (b s, 2H), 2.83 (t, $J = 8.8$ Hz, 2H), 1.66–1.79 (m, 2H), 1.43 (sxt, $J = 7.3$ Hz, 2H), 1.20–1.35 (m, 3H, impurity), 0.97 (t, $J = 7.3$ Hz, 3H), 0.90 (t, $J = 6.7$ Hz, 2H, impurity). ^{13}C NMR ($CDCl_3$) δ 166.3, 159.7, 141.1, 135.1 (impurity), 127.6 (impurity), 118.5, 105.5, 96.6, 36.7, 31.8 (impurity), 31.4, 29.0 (impurity), 22.6 (impurity), 22.4, 14.1 (impurity), 13.8.

4.1.20. 6-Amino-2-phenylnicotinonitrile (**41**)

38 (500 mg, 3.25 mmol), phenylboronic acid (595 mg, 4.88 mmol), K_3PO_4 (1.73 g, 8.14 mmol) and $Pd(PPh_3)_4$ (0.16 mmol) were added to a microwave vial together with toluene/EtOH (10:1, 11 mL). The vial was flushed with N_2, sealed and heated under microwave irradiation for 1 h at 100 °C. The reaction mixture was cooled to rt, 1 M NaOH (30 mL) was added, and the mixture was extracted with EtOAc (2 × 30 mL). The combined organic phase was dried over Mg_2SO_4 and evaporated under vacuum. Purification by DCVC (heptane/EtOAc 100:0 to 60:40) afforded the product as yellow solid (416 mg, 65%). mp 204.1–204.9 °C. ^1H NMR ($CDCl_3$) δ 7.89–7.83 (m, 2H), 7.75 (d, $J = 8.8$ Hz, 1H), 7.54–7.47 (m, 3H), 6.50 (d, $J = 8.8$ Hz, 1H). ^{13}C NMR (DMSO-d_6) δ 161.0, 141.6, 138.0, 129.5, 128.4, 128.2, 119.7, 106.6, 92.2.

4.1.21. 4-Chloro-5-iodopyridin-2-amine (**43**)

As described for **37** using 4-chloropyridin-2-amine **42** (4.93 g, 38.3 mmol), NIS (11.22 g, 49.9 mmol), and DMF (80 mL). Purification by DCVC afforded the product as orange solid (8.74 g, 90%). ^1H NMR ($CDCl_3$) δ 8.24 (s, 1H), 6.60 (s, 1H), 4.52 (bs, 1H). ^{13}C NMR ($CDCl_3$) δ 158.6, 156.2, 148.2, 109.3, 82.0.

4.1.22. 6-Amino-4-chloronicotinonitrile (**44**)

As described for **38** using **43** (8.58 g, 33.7 mmol), $Zn(CN_2)$ (2.38 g, 20.2 mmol), $Pd_2(dba)_3$ (1.54 g, 1.69 mmol), dppf (1.87 g, 3.37 mmol), and DMF/H_2O 99:1 (45 mL). Purification was attempted using DCVC (heptane/EtOAc/Et_3N 70:30:1 to 0:100:1 to EtOAc/MeOH 50:50) but the product is poorly soluble, and it was eluted from the column using MeOH. Some pure fractions of product were collected for characterization. Yield of impure product (6.86 g, >99%). mp (decomp.) >91 °C. ^1H NMR (DMSO-d_6) δ 8.37 (s, 1H), 7.37 (b s, 2H), 6.60 (s, 1H). ^{13}C NMR (DMSO-d_6) δ 154.9, 143.4, 116.2, 107.1, 95.5.

4.1.23. 6-Amino-4-ethylnicotinonitrile (**45**)

A flame-dried flask was charged with **44** (500 mg crude, max. 2.46 mmol), THF/NMP (10:1, 22 mL), and Fe(acac) (115 mg, 0.33 mmol). EtMgBr (3.0 M in Et_2O, 2.71 mL, 8.10 mmol) was added dropwise resulting in a colour change from red to brown to red/violet. The reaction mixture was stirred for 2 h at rt, then sat. aq.

NH_4Cl (50 mL) and EtOAc (50 mL) were added. The organic phase was separated, and the aqueous phase was extracted with EtOAc (50 mL). The combined organic phases were washed with brine (50 mL), dried over Mg_2SO_4, and evaporated under vacuum. Purification by DCVC (heptane/EtOAc 100:0 to 70:30) followed by recrystallization from MeOH afforded the product as white crystals (30 mg, 8% over two steps). mp 157.5–158.9 °C. ^{1}H NMR ($CDCl_3$) δ 8.30 (s, 1H), 6.37 (s, 1H), 4.89 (b s, 1H), 2.73 (q, J = 7.8 Hz, 2H), 1.28 (t, J = 7.8, 3H). ^{13}C NMR ($CDCl_3$) δ 160.4, 157.1, 153.6, 117.4, 106.7, 99.4, 27.1, 13.5.

4.1.24. 6-Amino-4-butylnicotinonitrile (**46**)

Preparation of Grignard reagent: To a two-necked flask containing Mg turnings (188 mg, 7.75 mmol) and THF (8.0 mL), BuBr (0.88 mL, 8.15 mmol) was added dropwise. The reaction did not start spontaneously upon addition of a few drops of BuBr, so a few iodine crystals were added, and the reaction mixture was heated using a heatgun. After the red colour of iodine had disappeared, the remaining BuBr was added dropwise. The reaction mixture was heated at 40–50 °C for 30 min then cooled to rt. Cross coupling was performed as described for **45** using **44** (1.00 g crude, max 4.91 mmol), Fe(acac) (230 mg, 0.65 mmol), and 2 consecutive additions of BuMgBr (1.0 M in THF, 16.3 mL, 16.3 mmol and 3.26 mL, 3.26 mmol). In the work-up the order of addition of sat. aq. NH_4Cl and EtOAC was reversed. Purification by DCVC (heptane/EtOAc 80:20) afforded the product as white solid (213 mg, 21% over two steps). mp 86.8–87.5 °C. ^{1}H NMR ($CDCl_3$) δ 8.46 (s, 1H), 8.22 (s, 1H), 8.05 (br s, 1H), 2.83 (m, 2H), 2.25 (s, 3H), 1.69 (m, 2H), 1.42 (sxt, J = 7.5 Hz, 2H), 0.97 (t, J = 7.5 Hz, 3H). ^{13}C NMR ($CDCl_3$) δ 168.9, 158.2, 153.6, 151.8, 116.2, 113.2, 34.3, 32.0, 24.9, 22.3, 13.7.

4.1.25. 6-Amino-4-phenylniconitrile (**47**)

Prepared as described for **41** using **44** (600 mg crude, max 2.95 mmol), phenylboronic acid (715 mg, 5.86 mmol), K_3PO_4 (2.07 g, 9.80 mmol), and $Pd(PPh_3)_4$ (226 mg, 0.20 mmol). The reaction mixture was heated at 100 °C for 2 h using microwave irradiation. Purification by DCVC (heptane/EtOAc 60:40 to 40:60) afforded the product as yellow solid (269 mg, 47% over two steps). mp 180.8–183.0 °C. ^{1}H NMR ($CDCl_3$) δ 8.45 (s, 1H), 7.61–7.46 (m, 5H), 6.55 (s, 1H), 5.02 (b s, 2H). ^{13}C NMR ($CDCl_3$) δ 161.32, 154.04, 151.19, 136.29, 128.79, 128.17, 127.46, 118.22, 107.05.

4.1.26. Methyl 6-amino-5-iodonicotinate (**49**)

Compound **48** (200 mg, 1.31 mmol) was dissolved in abs. EtOH (15 mL), I_2 (460 mg, 1.83 mmol) and $AgSO_4$ (572 mg, 1.83 mmol) were added in one portion. The reaction mixture was stirred at rt for 24 h then evaporated under vacuum. Purification by DCVC (CH_2Cl_2) afforded the product as off-white solid (208 mg, 57%). mp. 161–164 °C. ^{1}H NMR ($CDCl_3$) δ 8.65 (d, J = 2.1 Hz, 1H), 8.44 (d, J = 2.1 Hz, 1H), 5.45 (b s, 2H), 3.87 (s, 3H). ^{13}C NMR ($CDCl_3$) δ 165.1, 160.5, 151.1, 149.8, 148.3, 118.1, 52.4.

4.1.27. Methyl 6-amino-5-vinylnicotinate (**50**)

49 (291 mg, 1.04 mmol), potassium vinyltrifluoroborate (280 mg, 2.08 mmol), K_2CO_3 (3 M, 0.7 mL, 2.10 mmol), and $PdCl_2(PPh_3)_2$ (40 mg, 0.05 mmol) were added degassed toluene/H_2O (10:1, 55 mL). The reaction mixture was heated at 100 °C for 20 h then cooled to rt. Et_2O (100 mL) was added, and the organic phase was washed with H_2O (100 mL), sat. aq. $NaHCO_3$ (100 mL), and H_2O (100 mL). The organic phase was dried over Mg_2SO_4 and evaporated under vacuum. Purification by DCVC (heptane/EtOAc 4:1 to 2:1) afforded the product as white solid (75 mg, 40%). ^{1}H NMR ($CDCl_3$) δ 8.65 (d, J = 2.4 Hz, 1H), 8.06 (d, J = 2.4 Hz, 1H), 6.58 (dd, J = 17.1 Hz, J = 10.8 Hz, 1H), 5.74 (d, J = 17.1 Hz, 1H), 5.47 (d, J = 10.8 Hz, 1H), 3.89 (s, 3H). ^{13}C NMR ($CDCl_3$) δ 166.6, 159.0, 150.4, 136.2, 131.1, 118.9, 117.7, 117.0, 52.2.

4.1.28. Methyl 6-amino-5-ethylnicotinate (**51**)

50 (100 mg, 0.56 mmol) was dissolved in THF (6 mL), 10% Pd/C (50 mg) was added, and the solution was hydrogenated at rt for 16 h. The mixture was filtered through Celite, and the filtercake was washed with MeOH. The organic phase was evaporated, and purification by DCVC (EtOAc/heptane 1:2) afforded the product as white solid (94 mg, 93%). mp. 140–143 °C. ^{1}H NMR ($CDCl_3$) δ 8.59 (d, J = 2.1 Hz, 1H), 7.87 (d, J = 2.1 Hz, 1H), 4.97 (s, 2H), 3.87 (s, 3H), 2.46 (q, J = 7 Hz, 2H), 1.29 (t, J = 7 Hz, 3H). ^{13}C NMR ($CDCl_3$) δ 165.7, 155.6, 145.5, 133.4, 124.3, 113.3, 52.1, 23.7, 14.2.

4.2. Methods for pK_a determination of ionization constants

Titration was performed on a Sirius GLpKa Autotitrator (Sirius Analytical Instruments Ltd, East Sussex, UK). Depending on the structure two different detection techniques were used. If a compound changes UV–Vis absorption spectrum by the change of charge, a Diode array detector was used (compounds **3**,**24**,**26**). If no change in the UV–Vis absorption spectrum, traditional potentiometric detection was used (compounds **22**,**25**,**27**).

4.2.1. pK_a-determination by diode array detector [49]

The pK_a values were determined by a series of three titrations on a dilution of 50 μL 10 μM compound stock at 24 ± 1 °C and ion strength of 0.17 M using methanol as co-solvent. Methanol concentrations in the range 23–48% were used in the three titrations on each compound. The titrator was used in the mode with a diode-array-detector. This detector recorded the UV–Vis spectrum of the solution in-line, and thus the titration can be mapped via comparison to the spectra of the protonated and unprotonated species. The real aqueous pK_a-value was determined by extrapolation to zero-methanol content using a Yasuda–Shedlovsky plot.

4.2.2. pK_a-determination by potentiometric detection [49]

The pK_a values were determined by a series of three titration on approx. 2.5 mg compound at 24 ± 1 °C and ion strength of 0.17 M using methanol as co-solvent. Methanol concentrations in the range 23–48% were used in three titrations. A difference curve was created from each of these titrations by blank subtraction, and from these difference curves, methanol concentration dependent pK_a values were determined. The real aqueous pK_a-value was determined by extrapolation to zero-methanol content using a Yasuda–Shedlovsky plot.

4.3. Pharmacology

Characterization of **1**–**27** in muscimol binding: The binding assay was performed using rat brain synaptic membranes of cortex and the central hemispheres from male SPRD rats with tissue preparation as described in the literature [50]. On the day of the experiment, the membrane preparation was quickly thawed, homogenized in 50 volumes of ice-cold buffer (50 mM Tris–HCl buffer, pH 7.4), and centrifuged at 48,000*g* for 10 min at 4 °C. This washing step was repeated four times and the final pellet was resuspended in buffer. The assay was carried out in 96-wells plates, by incubation of membranes (70–80 μg protein) in 200 μL buffer, 25 μL [^{3}H]muscimol (5 nM final concentration), and 25 μL test substance in various concentrations, for 60 min at 0 °C. The reaction was terminated by rapid filtration through GF/C filters (Perkin Elmer Life Sciences), using a 96 well Packard FilterMate cell-harvester, followed by washing with 3 × 250 μL of ice-cold buffer. The dried filters were added Microscint scintillation fluid (Perkin

Elmer Life Sciences), and the amount of filterbound radioactivity was quantified in a Packard TopCount microplate scintillator counter. The experiments were performed in triplicate at least three times for each compound. Non-specific binding was determined using 1.0 mM GABA. The binding data was analyzed by a non-linear regression curve-fitting procedure using GraphPad Prism v. 6.00 (GraphPad Software, CA, USA). IC_{50} values were calculated from inhibition curves and converted to K_i values using the modified Cheng–Prusoff equation [51].

Functional characterization in the FMP assay: The functional characterization of compounds **3**, **9**–**11**, **14**–**16**, **22**, **23**, **25**, **27** at $GABA_A$Rs in the FLIPR™ Membrane Potential Blue assay was performed essentially as described previously [52]. 8×10^5 tsA-201 cells were split into a 6 cm tissue culture plate and transfected the following day with a total of 5 μg cDNA using Polyfect (Qiagen, Hilden, Germany). Cells were co-transfected with 1 μg $\alpha_{1,2,3,5}$-pcDNA3.1, 1 μg β_2-pcDNA3.1 and 3 μg γ_{2S}-pCDNA3.1, or transfected with 5 μg ρ_1-pcDNA3. The following day, cells were split into poly-D-lysine-coated black 96-wells plates with clear bottom (BD Biosciences, Bedford, MA). 16–24 h later the medium was aspirated, and the cells were washed with 100 μL Krebs buffer [140 mM NaCl/4.7 mM KCl/2.5 mM $CaCl_2$/1.2 mM $MgCl_2$/11 mM HEPES/10 mM D-Glucose, pH 7.4]. 50 μL Krebs buffer was added to the wells (in the antagonist experiments, various concentrations of the antagonist were dissolved in the buffer) and then an additional 50 μL Krebs buffer supplemented with assay dye (1 mg/mL) was added to each well. Then the plate was incubated at 37 °C in a humidified 5% CO_2 incubator for 30 min and assayed in a NOVOstar™ plate reader (BMG Labtechnologies, Offenburg, Germany) measuring emission [in fluorescence units (FU)] at 560 nm caused by excitation at 530 nm before and up to 1 min after addition of 33 μL agonist solution. The experiments were performed in duplicate at least three times for each compound at each receptor. EC_{70}–EC_{90} concentrations of GABA were used as agonist in the antagonist experiments. Concentration–response curves for agonists and concentration–inhibition curves for antagonists were constructed based in the difference in the fluorescence units (△FU) between the maximal fluorescence recording made before and after addition of agonist obtained for different concentrations of the respective ligands. The curves were generated by nonweighted least-squares fits using the program KaleidaGraph 3.6 (Synergy Software).

4.4. Computational chemistry

4.4.1. Ligand docking

The full-length homology model of the α1β2γ2 GABA receptor developed by Bergmann et al. [20] was used for generating binding mode hypotheses. Compounds **3**, **11**–**13**, **15**–**16**, **22**, **25** and **27** were docked into the GABA binding site between chains A and B using the Induced Fit Docking protocol in Schrodinger's Maestro v9.5 [53]. Amino acid residues in an 8 Å distance from the docked ligands were sampled and otherwise default settings were used. Poses were filtered on the basis of having a GABA like hydrogen-bonding pattern, with hydrogen bonds from the carboxylate group to α_1Arg66, α_1Thr129 and β_2Thr202, and hydrogen bonds from the amidine group to β_2Glu155, and the backbone carbonyl of β_2Ser156 and β_2Tyr157. A table showing docking scores is provided as supporting information (SI Table S.1).

4.4.2. GRID

Molecular interaction fields were calculated for the homology model using the methyl (C3) probe and 3 planes per Angstrom using the Molecular Discovery's GRID v22c program [54,55]. The obtained molecular interaction fields were converted to the .xplor file format using the included k2f utility and visualized in PyMOL [56].

4.4.3. Molecular mechanics energy calculations

The relative potential energy of the torsional angle between the carboxylate group and the pyridine/piperidine ring of **3** and **22** was estimated based on a coordinate scan performed using MacroModel v.10.1 [57], the OPLS_2005 force field, and water solvent model. The energy scan increment was set to 10° and otherwise default settings were used.

Acknowledgements

We thank Shahrokh Pradah for technical laboratory assistance and H. Lundbeck A/S for pK_a determination. J.G.P. was supported by the Lundbeck and Carlsberg Foundations, T.S. was supported by the Danish Research Council, R.B. was supported by the Velux Foundation. A.A.J. was supported by the Novo Nordisk Foundation.

Appendix A. Supplementary data

Supplementary data related to this article can be found at http://dx.doi.org/10.1016/j.ejmech.2014.07.039.

References

[1] A.C. Foster, J.A. Kemp, Glutamate- and GABA-based CNS therapeutics, Curr. Opin. Pharmacol. 6 (2006) 7–17.
[2] G.A.R. Johnston, $GABA_A$ receptor channel pharmacology, Curr. Pharm. Des. 11 (2005) 1867.
[3] W. Sieghart, G. Sperk, Subunit composition, distribution and function of $GABA_A$ receptor subtypes, Curr. Top. Med. Chem. 2 (2002) 795–816.
[4] W. Paul J., $GABA_A$ receptor subtypes in the brain: a paradigm for CNS drug discovery? Drug Discov. Today 8 (2003) 445–450.
[5] A.R.J. Graham, C. Mary, R.H. Jane, N.M. Kenneth, $GABA_C$ receptors as drug targets, Curr. Drug Targets: CNS Neurol. Disord. 2 (2003) 260–268.
[6] J.G. Petersen, R. Bergmann, P. Krogsgaard-Larsen, T. Balle, B. Frølund, Probing the orthosteric binding site of GABAA receptors with heterocyclic GABA carboxylic acid bioisosteres, Neurochem. Res. 39 (2014) 1005–1015.
[7] G.A.R. Johnston, D.R. Curtis, W.C. de Groat, A.W. Duggan, Central actions of ibotenic acid and muscimol, Biochem. Pharmacol. 17 (1968) 2488–2489.
[8] P. Krogsgaard-Larsen, G.A.R. Johnston, Structure-activity studies on the inhibition of GABA binding to rat brain membranes by muscimol and related compounds, J. Neurochem. 30 (1978) 1377–1382.
[9] P. Krogsgaard-Larsen, G.A.R. Johnston, D. Lodge, D.R. Curtis, A new class of GABA agonist, Nature 268 (1977) 53–55.
[10] U. Kristiansen, J.D.C. Lambert, E. Falch, P. Krogsgaard-Larsen, Electrophysiological studies of the $GABA_A$ receptor ligand, 4-PIOL, on cultured hippocampal neurones, Br. J. Pharmacol. 104 (1991) 85–90.
[11] J.R. Byberg, I.M. Labouta, E. Falch, H. Hjeds, P. Krogsgaard-Larsen, Synthesis and biological activity of a $GABA_A$ agonist which has no effect on benzodiazepine binding and of structurally related glycine antagonists, Drug Des. Deliv. 1 (1987) 261–274.
[12] B. Frølund, A.T. Jørgensen, L. Tagmose, T.B. Stensbøl, H.T. Vestergaard, C. Engblom, U. Kristiansen, C. Sanchez, P. Krogsgaard-Larsen, T. Liljefors, Novel class of potent 4-arylalkyl substituted 3-isoxazolol $GABA_A$ antagonists: synthesis, pharmacology, and molecular modeling, J. Med. Chem. 45 (2002) 2454–2468.
[13] B. Frølund, L. Tagmose, T. Liljefors, T.B. Stensbøll, C. Engblom, U. Kristiansen, P. Krogsgaard-Larsen, A novel class of potent 3-isoxazolol $GABA_A$ antagonists: design, synthesis, and pharmacology, J. Med. Chem. 43 (2000) 4930–4933.
[14] K. Brejc, W.J. van Dijk, R.V. Klaassen, M. Schuurmans, J. van der Oost, A.B. Smit, T.K. Sixma, Crystal structure of an ACh-binding protein reveals the ligand-binding domain of nicotinic receptors, Nature 411 (2001) 269–276.
[15] S.B. Hansen, T.T. Talley, Z. Radic, P. Taylor, Structural and ligand recognition characteristics of an acetylcholine-binding protein from Aplysia californica, J. Biol. Chem. 279 (2004) 24197–24202.
[16] P.H.N. Celie, R.V. Klaassen, S.E. van Rossum-Fikkert, R. van Elk, P. van Nierop, A.B. Smit, T.K. Sixma, Crystal structure of acetylcholine-binding protein from Bulinus truncatus reveals the conserved structural scaffold and sites of variation in nicotinic acetylcholine receptors, J. Biol. Chem. 280 (2005) 26457–26466.
[17] R.E. Hibbs, E. Gouaux, Principles of activation and permeation in an anion-selective Cys-loop receptor, Nature 474 (2011) 54–60.
[18] R.J.C. Hilf, R. Dutzler, X-ray structure of a prokaryotic pentameric ligand-gated ion channel, Nature 452 (2008) 375–379.

[19] N. Bocquet, H. Nury, M. Baaden, C. Le Poupon, J.-P. Changeux, M. Delarue, P.-J. Corringer, X-ray structure of a pentameric ligand-gated ion channel in an apparently open conformation, Nature 457 (2009) 111–114.
[20] R. Bergmann, K. Kongsbak, P.L. Sørensen, T. Sander, T. Balle, A unified model of the $GABA_A$ receptor comprising agonist and benzodiazepine binding sites, PLoS One 8 (2013) e52323.
[21] T. Sander, B. Frølund, A.T. Bruun, I. Ivanov, J.A. McCammon, T. Balle, New insights into the $GABA_A$ receptor structure and orthosteric ligand binding: receptor modeling guided by experimental data, Proteins Struct. Funct. Bioinf. 79 (2011) 1458–1477.
[22] J.G. Petersen, R. Bergmann, H.A. Møller, C.G. Jørgensen, B. Nielsen, J. Kehler, K. Frydenvang, J. Kristensen, T. Balle, A.A. Jensen, U. Kristiansen, B. Frølund, Synthesis and biological evaluation of 4-(aminomethyl)-1-hydroxypyrazole analogues of muscimol as γ-aminobutyric acid(A) receptor agonists, J. Med. Chem. 56 (2013) 993–1006.
[23] P.E. Maligres, M.S. Waters, F. Fleitz, D. Askin, A highly catalytic robust palladium catalyzed cyanation of aryl bromides, Tetrahedron Lett. 40 (1999) 8193–8195.
[24] J. Magano, A. Acciacca, A. Akin, B.M. Collman, B. Conway, M. Waldo, M.H. Chen, K.E. Mennen, The synthesis of a dopamine D_2 partial agonist for the treatment of schizophrenia, Org. Process Res. Dev. 13 (2009) 555–566.
[25] P. Eastwood, J. Gonzalez, S. Paredes, A. Nueda, T. Domenech, J. Alberti, B. Vidal, Discovery of N-(5,6-diarylpyridin-2-yl)amide derivatives as potent and selective A_{2B} adenosine receptor antagonists, Bioorg. Med. Chem. Lett. 20, 1697–1700.
[26] J.L. Bolliger, M. Oberholzer, C.M. Frech, Access to 2-aminopyridines – compounds of great biological and chemical significance, Adv. Synth. Catal. 353, 945–954.
[27] A. Fürstner, A. Leitner, Iron-catalyzed cross-coupling reactions of alkylgrignard reagents with aryl chlorides, tosylates, and triflates, Angew. Chem. Int. Ed. 41 (2002) 609–612.
[28] C. Koradin, W. Dohle, A.L. Rodriguez, B. Schmid, P. Knochel, Synthesis of polyfunctional indoles and related heterocycles mediated by cesium and potassium bases, Tetrahedron 59 (2003) 1571–1587.
[29] P.G. Dunbar, G.J. Durant, T. Rho, B. Ojo, J.J. Huzl III, D.A. Smith, A.A. El-Assadi, S. Sbeih, D.O. Ngur, Design, synthesis, and neurochemical evaluation of 2-amino-5-(alkoxycarbonyl)-3,4,5,6-tetrahydropyridines and 2-Amino-5-(alkoxycarbonyl)-1,4,5,6-tetrahydropyrimidines as M1 muscarinic receptor agonists, J. Med. Chem. 37 (1994) 2774–2782.
[30] D. Cartwright, J.R. Ferguson, T. Giannopoulos, G. Varvounis, B.J. Wakerfield, Synthesis of some β-trichloromethyl-azines and -diazines, J. Chem. Soc. Perkin Trans. 1 (1995) 2595–2597.
[31] B. Ebert, M. Mortensen, S.A. Thompson, J. Kehler, K.A. Wafford, P. Krogsgaard-Larsen, Bioisosteric determinants for subtype selectivity of ligands for heteromeric $GABA_A$ receptors, Bioorg. Med. Chem. Lett. 11 (2001) 1573–1577.
[32] P. Krogsgaard-Larsen, H. Hjeds, E. Falch, F.J. Jørgensen, L. Nielsen, Recent advances in GABA agonists, antagonists and uptake inhibitors: structure-activity relationships and therapeutic potential, Adv. Drug Res. (1988) 382–456.
[33] P. Krogsgaard-Larsen, H. Hjeds, D.R. Curtis, J.D. Leah, M.J. Peet, Glycine antagonists structurally related to muscimol, THIP, or isoguvacine, J. Neurochem. 39 (1982) 1319–1324.
[34] A. Neu, H. Neuhoff, G. Trube, S. Fehr, K. Ullrich, J. Roeper, D. Isbrandt, Activation of $GABA_A$ receptors by guanidinoacetate: a novel pathophysiological mechanism, Neurobiol. Dis. 11 (2002) 298–307.
[35] M. Chebib, N. Gavande, K. Wong, A. Park, I. Premoli, K. Mewett, R. Allan, R. Duke, G. Johnston, J. Hanrahan, Guanidino acids act as ρ1 $GABA_C$ receptor antagonists, Neurochem. Res. 34 (2009) 1704–1711.
[36] M.M. Campbell, S.J. Mickel, G. Singh, (±)-2-Amino-2-thiazoline-4-ethanoic acid; a novel, specific $GABA_A$ receptor agonist, Bioorg. Med. Chem. Lett. 1 (1991) 247–248.
[37] C.G. Wermuth, J.J. Bourguignon, G. Schlewer, J.P. Gies, A. Schoenfelder, A. Melikian, M.J. Bouchet, D. Chantreux, J.C. Molimard, Synthesis and structure-activity relationships of a series of aminopyridazine derivatives of γ-aminobutyric acid acting as selective $GABA_A$ antagonists, J. Med. Chem. 30 (1987) 239–249.
[38] D. Krehan, S. í Storustovu, T. Liljefors, B. Ebert, B. Nielsen, P. Krogsgaard-Larsen, B. Frølund, Potent 4-arylalkyl-substituted 3-isothiazolol $GABA_A$ competitive/noncompetitive antagonists: synthesis and pharmacology, J. Med. Chem. 49 (2006) 1388–1396.
[39] C.L. Padgett, A.P. Hanek, H.A. Lester, D.A. Dougherty, S.C. Lummis, Unnatural amino acid mutagenesis of the GABA(A) receptor binding site residues reveals a novel cation-pi interaction between GABA and beta 2Tyr97, J. Neurosci. 27 (2007) 886–892.
[40] J.G. Newell, R.A. McDevitt, C. Czajkowski, Mutation of glutamate 155 of the GABAA receptor beta2 subunit produces a spontaneously open channel: a trigger for channel activation, J. Neurosci. 24 (2004) 11226–11235.
[41] W. Haefliger, L. Révész, R. Maurer, D. Römer, H.-H. Büscher, Analgesic GABA agonists. Synthesis ans structure-activity studies on analogues and derivatives of muscimol and THIP, Eur. J. Med. Chem. 19 (1984) 149–156.
[42] E. Falch, P. Jacobsen, K.-L. P., Synthesis, GABA agonist activity and effects on GABA and diazepam binding of some N-substituted analogues of GABA 20 (1985) 447–453.
[43] B. Ebert, S.A. Thompson, K. Saounatsou, R. McKernan, P. Krogsgaard-Larsen, K.A. Wafford, Differences in agonist/antagonist binding affinity and receptor transduction using recombinant human γ-aminobutyric acid type a receptors, Mol. Pharmacol. 52 (1997) 1150–1156.
[44] B. Ebert, K.A. Wafford, P.J. Whiting, P. Krogsgaard-Larsen, J.A. Kemp, Molecular pharmacology of gamma-aminobutyric acid type A receptor agonists and partial agonists in oocytes injected with different alpha, beta, and gamma receptor subunit combinations, Mol. Pharmacol. 46 (1994) 957–963.
[45] J.R. Atack, $GABA_A$ receptor subtype-selective efficacy: TPA023, an α2/α3 selective non-sedating anxiolytic and α5IA, an α5 selective cognition enhancer, CNS Neurosci. Ther. 14 (2008) 25–35.
[46] M. Farrant, Z. Nusser, Variations on an inhibitory theme: phasic and tonic activation of GABA(A) receptors, Nat. Rev. Neurosci. 6 (2005) 215–229.
[47] N. Collinson, F.M. Kuenzi, W. Jarolimek, K.A. Maubach, R. Cothliff, C. Sur, A. Smith, F.M. Otu, O. Howell, J.R. Atack, R.M. McKernan, G.R. Seabrook, G.R. Dawson, P.J. Whiting, T.W. Rosahl, Enhanced learning and memory and altered GABAergic synaptic transmission in mice lacking the alpha 5 subunit of the GABAA receptor, J. Neurosci. 22 (2002) 5572–5580.
[48] D.S. Pedersen, C. Rosenbohm, Dry column vacuum chromatography, Synthesis (2001) 2431–2434.
[49] J. Comer, Ionization constants and ionization profiles, in: D.J. Triggle, J.B. Taylor (Eds.), Comprehensive Medicinal Chemistry II, Elsevier, Oxford, 2006, pp. 357–397.
[50] R.W. Ransom, N.L. Stec, Cooperative modulation of [^{3}H]MK-801 binding to the N-methyl-d-aspartate receptor-ion channel complex by l-glutamate, glycine, and polyamines, J. Neurochem. 51 (1988) 830–836.
[51] P. Leff, I.G. Dougall, Further concerns over Cheng-Prusoff analysis, Trends Pharmacol. Sci. 14 (1993) 110–112.
[52] C. Madsen, A.A. Jensen, T. Liljefors, U. Kristiansen, B. Nielsen, C.P. Hansen, M. Larsen, B. Ebert, B. Bang-Andersen, P. Krogsgaard-Larsen, B. Frolund, 5-Substituted imidazole-4-acetic acid analogues: synthesis, modeling, and pharmacological characterization of a series of novel gamma-aminobutyric acid(C) receptor agonists, J. Med. Chem. 50 (2007) 4147–4161.
[53] 2013-2, I.F.D. p. Glide Version 5.9, Prime Version 3.2, Schrödinger, LLC, New York, NY, 2013.
[54] P.J. Goodford, A computational procedure for determining energetically favorable binding sites on biologically important macromolecules, J. Med. Chem. 28 (1985) 849–857.
[55] Molecular Discovery L, G., Pinner, Middelsex, UK, 2005.
[56] The PYMOL Molecular Graphics System, Version 1.6.0.0., L. Schrödinger, LLC.
[57] MacroModel v. 10.1, L. Schrödinger, N.Y., NY, 2013.
[58] P. Krogsgaard-Larsen, L. Nielsen, E. Falch, D.R. Curtis, GABA agonists. Resolution, absolute stereochemistry and enantioselectivity of (*S*)-(+)- and (*R*)-(-) dihydromuscimol, J. Med. Chem. 28 (1985) 1612–1617.